JACS
JOURNAL OF THE AMERICAN CHEMICAL SOCIETY
pubs.acs.org/JACS

Article

Photoisomerization Paths of α,ω-Diphenylpolyenes: Reaction Rate Dependence on Temperature, Excitation Wavelength, and Deuteration

Alexander L. Dobryakov, Daria Schriever, Martin Quick, J. Luis Pérez-Lustres, Ilya N. Ioffe, and Sergey A. Kovalenko*

Cite This: J. Am. Chem. Soc. 2024, 146, 32463−32478

Read Online

ACCESS | Metrics & More | Article Recommendations | Supporting Information

ABSTRACT: The photoisomerization rate k_{iso} of *trans*-stilbene (tS) and trans−trans-diphenylbutadiene (ttD) is studied in solution and compared to that in jet/gas. Rice−Ramsperger−Kassel−Marcus (RRKM) theory correctly predicts the tS rate in jet, $k_{RRKM} = A_m \exp(-E_{in}/kT_m)$ with E_{in} = 1398 cm^{-1}, and A_m = 1.8 ps^{-1} corresponding to frequency ν_{iso} = 60 cm^{-1} of the reactive mode, T_m being the molecular temperature. However, the behavior in solution cannot be explained by the RRKM rate alone. In solution the rate $k_{iso} = A_S \exp(-E_b/kT_S)$ has a similar form, but depends mainly on solvent temperature T_S and proceeds much faster, A_S = 19 ps^{-1}, E_b = 1520 cm^{-1} in *n*-hexane. Moreover, excitation at high excess energy, resulting in molecular temperature T_m = 607 K, affects the rate only slightly, unlike in jet, and contrary to common theoretical models. The experimental results clearly indicate two isomerization paths in solution: via relatively slow intramolecular activation $A_m \sim 1$ ps^{-1}, and by much faster solvent activation A_S = 18 ps^{-1} due to solute−solvent interactions (collisions). The data in *n*-alkanes confirm previously established power dependence $k_{iso} \sim \eta^{\alpha}$ on viscosity η, with α = 0.30 for tS, and α = 0.35 for ttD. With E_η being the viscosity barrier, its contribution to E_b can be isolated, giving the intramolecular barrier $E_{in} = (E_b - \alpha E_\eta)$, slightly lower than in jet/gas, probably due to the dispersive/induction interactions in solution.

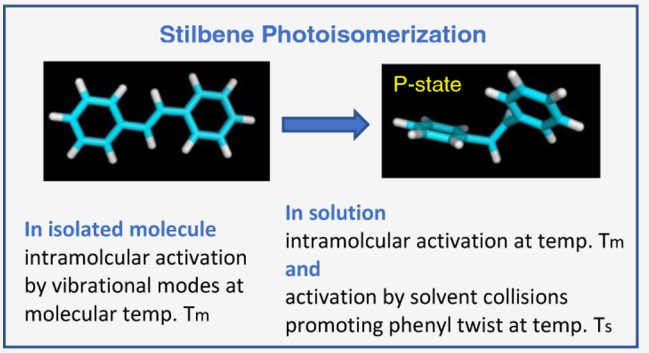

1. INTRODUCTION

The photoisomerization of *trans*-stilbene (tS)[1−28] and trans−trans-diphenylbutadiene (ttD)[29−42] has long been in the focus of research. The probes were carefully investigated in the gas and liquid phase, both experimentally[1−42] and theoretically.[3,8,19,43−55] An account on work before 1991 is given in refs13,17,34, and some recent results are reviewed in ref 56. It is currently well established that the isomerization proceeds via phenyl torsion around the ethylenic bond. Upon $S_0 \rightarrow S_1$ optical excitation, the molecule twists over a barrier to perpendicular conformation *P*, and then relaxes through a conical intersection to ground state S_0, completing the twist with cis or trans isomer.

The isomerization path and the intermediate *P*-state was proposed by Saltiel in 1967,[1] and later received a solid theoretical justification.[3,48,50,52,53] It was originally called a "phantom state" because of the difficulty for detection. Indeed, it took 40 years to observe and spectroscopically identify it first in jet[23] and then in solution.[24] The problem was related with its very short, ∼0.1 ps lifetime, lack of emission, and with that the *P* absorption band lay in the UV, not easily accessible in earlier studies. With the progress in ultrafast pulses, and especially in broadband transient absorption spectroscopy,[57] it became possible to cover the UV range, while keeping a sub-0.1 ps resolution.[24] Later on, a better record of *P* was achieved with 1,1′-stilbene derivatives in which the *P*-state is long-lived, up to 100 ps.[25]

Starting from early studies, a major challenge was to test Rice−Ramsperger−Kassel−Marcus (RRKM)[3,19,58] and Kramers[59,60] theory of unimolecular reactions. At rather general conditions,[3,19] the RRKM theory predicts an isomerization rate k_{iso} in a simple Arrhenius form

$$k_{iso} = k_{RRKM} = c\nu_{iso} \exp(-E_b/kT) \quad (1)$$

where ν_{iso} in cm^{-1} is the frequency of the reaction mode, E_b − isomerization barrier, k − Boltzmann constant, T − temperature, c − velocity of light. To be applicable eq 1 requires fast intramolecular vibrational redistribution (IVR), $k_{IVR} \gg k_{iso}$,

Received: July 7, 2024
Revised: October 29, 2024
Accepted: October 29, 2024
Published: November 12, 2024

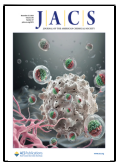

https://doi.org/10.1021/jacs.4c09134
J. Am. Chem. Soc. 2024, 146, 32463−32478

and low-frequency isomerization mode $\nu_{iso} \ll kT$. When $\nu_{iso} > kT$, the preexponential factor $A = c\nu_{iso}$ is more complex, although still applicable for crude estimates.[3]

Jet experiments on tS at low excess excitation energy reported $k_{iso} \sim 1$ ns^{-1}, $E_b \approx 1200$ cm^{-1}.[8−11] A similar barrier E_b was also measured in hydrocarbon solution.[2,13,16] Assuming the reaction frequency ν_{iso} to be independent of the environment, one may expect a comparable photoisomerization rate, however the rate in solution is in fact 1 order of magnitude higher. For example, in *n*-hexane at 293 K, $k_{iso} > 10$ ns^{-1}.[13] Moreover, measurements in buffer gases[14,18] revealed a linear rise of k_{iso} with the buffer pressure, thus directly indicating a crucial role of solute−solvent collisions in promoting the reaction.

There are basically two ways to resolve the dilemma. The first, and currently widely accepted, is that IVR is presumably slow (restricted) at collision less conditions. It limits the energy flow from intramolecular bath to reaction mode, and hence slows down the isomerization rate in jet and low-pressure gases. Once the reaction depopulates the transition state, the slow IVR cannot repopulate it sufficiently fast. By adding a buffer gas, collisions with tS molecules accelerate IVR, and at high-pressure the IVR becomes fast enough to not limit the reaction rate anymore. Early computations reported the reaction frequency ν_{iso} in the range 400−600 cm^{-1},[10,17,43,47,48] thus supporting the hypothesis of slow IVR. Indeed, with $\nu_{iso} = 600$ cm^{-1} it was possible to fit the reaction rate k_{iso} both in solution and in buffer gases at different pressures.[48,51] It is worth noting that with the barrier $E_b \approx 1200$ cm^{-1},[8−11] the choice $\nu_{iso} \sim 600$ cm^{-1} is enforced to match the rate in solution by the RRKM theory.

An alternative solution is to assume that solute−solvent collisions directly activate[14,21,27] the reactive mode ν_{iso} in addition to intramolecular activation. In 1986 Balk and Fleming[14] mentioned such a mechanism but abandoned it as inconsistent with the RRKM approach. Instead, they supported the restricted IVR hypothesis.[14,15,43,47,48]

Note that restricted IVR was questioned in 1996 by Zewail and co-workers[11] who inferred for tS in jet $k_{IVR} > 1$ ps$^{-1} \gg k_{iso}$ at $T = 293$ K. But proponents of the limited IVR[43,47,48,51,54,55] put forward a much stronger requirement, $k_{IVR} \gg c\nu_{iso}$, with $\nu_{iso} = 600$ cm^{-1} resulting in $k_{IVR} \gg 18$ ps^{-1}.[47,48,51] However, Troe and co-workers[19] demonstrated in 2002 that the complete IVR is consistent with the results in jet.[11] They successfully fitted the data by the RRKM rate, eq 1 with $\nu_{iso} = 24$ cm^{-1} and $E_b = 1155$ cm^{-1}. Recent quantum chemical computations[52,53] likewise support $\nu_{iso} \sim 30$ cm^{-1}. Regarding the rate in solution, Troe and co-workers concluded that "the trans-stilbene enigma of an order of magnitude discrepancy between thermally averaged gas-phase rate and low viscosity liquid-phase rate remains unresolved"[19] thus leaving the problem for future work.

Kramers[59] in 1940 considered the viscosity effect on the unimolecular reaction rate. At very low viscosity η the Kramers theory[59,60] predicts $k_{Kram} \sim \eta$, and for higher η the rate is expressed as

$$k_{Kram}(\eta) = \kappa(\eta) c\nu_{iso} \exp(-E_b/kT) \quad (2)$$

where coefficient $\kappa(\eta)$ is given by

$$\kappa(\eta) = [(x^2 + 1)^{1/2} - x] \quad \text{with} \quad x = C\eta/2\nu_b \quad (3)$$

Here C is a constant, and ν_b the reaction frequency at the barrier top. When $x \ll 1$ the viscosity is still small and the RRKM rate k_{RRKM} is recovered. For high viscosity, $x \gg 1$, $\kappa \approx 1/2x$ and $k_{Kram} \sim k_{RRKM}/\eta$ is inversely proportional to η, that seems reasonable in the liquid phase. There were numerous attempts to fit the photoisomerization rate k_{iso} of α,ω-diphenylpolyenes by the Kramers eq 2, but only with a partial success.[6,12,29,33,37,38]

It is worth mentioning an important difference between tS and ttD regarding their electronic level structure. For tS the lowest S_1 state is always 1^1B_u both in gas and liquid.[49,52,53] However, this is not the case for ttD, its S_1 state in gas is 2^1A_g[32] and switches to 1^1B_u in solution.[38−41] Therefore, a comparison of gas- and solution-phase isomerization rate of ttD is meaningless. Nonetheless, a comparison between the rates of tS and ttD in solution is in order, as the isomerization proceeds from the same 1^1B_u state of similar electronic structure. For higher α,ω-diphenylpolyenes, the dark 2^1A_g becomes the lowest S_1 state also in solution[34] complicating spectroscopy of these probes. In this regard the photochemistry of stilbene is unique among α,ω-diphenylpolyenes.

Next important note concerns the rate dependence k_{iso} on the excitation wavelength λ_{exc}. In jet/gas at collisionless conditions, the dependence on λ_{exc} is very pronounced,[11] while in solution it is rather weak. This was naturally ascribed to rapid solute−solvent energy transfer,[6,12] but the consequences for the RRKM and Kramers model were not recognized until 2013.[27] Briefly, the point is as follows. For a molecule excited high above the 0−0 transition, intramolecular vibrational energy increases resulting in high molecular temperature T_m. In jet/gas at collisionless conditions T_m remains constant during the isomerization, while in solution the molecule cools down by surrounding solvent molecules to solvent temperature T_S. The cooling dynamics is currently well-known.[20−22] In particular for tS in aprotic solvents, the cooling time τ_c is about 10 ps[22] that can be easily resolved by modern ultrafast techniques. Consequently, as isomerization and vibrational cooling of tS occur on a comparable time scale, one has to consider the effect of time-dependent molecular temperature $T_m(t)$ on the isomerization rate k_{iso}. That is, one has to measure $k_{iso}(t)$ and compare it to $k_{RRKM}(t)$ or $k_{Kram}(t)$, eqs 1 or 2, under condition of nonstationary $T_m(t)$.

An important piece of information can be obtained with deuterated probes. For tS the rate k_{iso} was measured and calculated for various deuteration patterns: at the ethylenic bond (D2), phenyl rings (D10), and with full deuteration (D12).[10,15,17,19,43,44,48] Interestingly, the behavior in jet was qualitatively different from that in buffer gases or in solution. In jet, the rate gradually decreased in the order D0 (nondeuterated), D10, D2, D12, while in solution the rate is the same in D0 and D10, and in D2 and D12, being 1.4 times higher in the former pair.

A theoretical consideration of the photoisomerization path suggests either the commonly assumed twisting motion aka one-bond flip, or various hula-twist/bicycle-pedal mechanisms[23] which do not involve any significant displacement of bulky phenyl rings, and thus might be possible even in solid matrices. However, there is no evidence that such a motion is realized in stilbene or diphenylbutadiene. Recent computations on cis,cis-diphenylbutadiene in crystalline environment predicts an activation energy of 10,000 cm^{-1},[61] much higher than the isomerization barrier observed for tS o ttD in solution. Thus, the twisting photoisomerization pathway can be

https://doi.org/10.1021/jacs.4c09134
J. Am. Chem. Soc. 2024, 146, 32463−32478

regarded as prevailing, and quantum chemistry helps to understand it in detail, at least in the gas phase.[53] In solution, however, although the qualitative isomerization picture is likely the same, quantitative simulations of the excited-state evolution are challenging. Indeed, in the *P*-state region of S_1, a very strong spontaneous polarization develops, and at the same time there is a need to account for both static and dynamic electronic correlation. On the contrary, the Franck−Condon S_1-state is nonpolar and dominated by a single HOMO−LUMO excitation. Hence, the solvent field should lower the barrier due to high polarity of the *P*-state. Simulations of the deuteration effects on the isomerization rate in excited tS by the transition state theory (TST), thus implying complete IVR,[53] have been found to agree with the above experimental liquid-phase picture.

All the issues outlined above are addressed in the present paper. Broadband transient absorption spectroscopy is applied to measure the photoisomerization rates k_{iso} of tS and ttD in solution at different solvent temperature T_S and viscosities. In addition, the dependence on excitation wavelengths λ_{exc}, that is on molecular temperature T_m, is measured and analyzed. Finally, the rate dependence on the deuteration pattern is also measured and discussed. The results are compared to those in jet/gas.[11] We show that the RRKM theory works well in jet/gas at collisionless conditions but fails to explain the behavior in solution. Here we suggest a new isomerization mechanism involving solvent collisions with the solute phenyl ring.

2. METHODS

2.1. Quantum Chemical Calculations. The S_1 and S_2 states of ttD are computed with the Firefly quantum chemistry package, version 8.2.1,[62] partly based on the GAMESS(US)[63] source code. We employ the XMCQDPT2[64] multiconfiguration quasi-degenerate perturbation theory previously applied by us to tS.[53] The (12e,12o) active space includes all π and π^* orbitals except for two lowest and two highest ones. In order to cover the major contributions to S_1 and S_2 as revealed by the PT2 treatment, the state-averaging at the CASSCF level includes seven lowest roots. The XMCQDPT2 model space further encompasses 12 additional roots to ensure convergence of geometry optimizations across the potential energy surfaces. At the PT2 level, the chemical core is frozen, and an intruder state avoidance (ISA) shift of 0.02 au is applied. The Def2-TZVPP basis set is used.

2.2. Experiment. The transient absorption setup[57,65] with applications[22,24−28,41,42] has been described elsewhere. Transient absorption (TA) spectra of tS and ttD are measured in the spectral range 275−690 nm. Magic angle signal $\Delta A = (\Delta A_{\parallel} + 2\Delta A_{\perp})/3$ is calculated from parallel $\Delta A_{\parallel}$ and perpendicular $\Delta A_{\perp}$ polarization. The temporal instrument response is 0.1 ps broad. Multiple 10−20 pump−probe scans are applied to improve the signal-to-noise ratio. Transient anisotropy ρ is given by

$$\rho(\lambda, t) = (\Delta A_{\parallel} - \Delta A_{\perp})/(3\Delta A) \quad (4)$$

The anisotropy decay $\rho(t)$ is fitted monoexponentially to give the rotational diffusion time τ_R (or simply rotational time for brevity).

Absorption spectra of tS and ttD in *n*-hexane are shown in Figure 1. In TA measurements, absorbance at λ_{exc} was less than 0.5. A 30 mL solution of 0.1−0.2 mg/mL of tS or ttD was flown through a temperature-stabilized cell of 0.3 mm internal thickness. The pump and probe beams were focused onto the cell at 15° to 0.1 mm spots.

3. RESULTS

The plan of this section is as follows. First, we explain how the isomerization rate k_{iso} is extracted from broadband TA measurements. Then, viscosity- and temperature-dependent isomerization time $\tau_{iso} = 1/k_{iso}$ and rotational time τ_R is used to obtain the viscosity contribution E_η to isomerization barrier E_b. This results in intramolecular barrier E_{in} in solution that can then be compared to the gas phase barrier. We also consider the isoviscosity rates for obtaining E_{in} and conclude that they overestimate the intramolecular barriers. Finally, we present the isomerization kinetics recorded at high excess vibrational energy (λ_{exc} = 267 nm for tS and λ_{exc} = 284 nm for ttD) resulting in hot probe molecules, $T_m \sim 600$ K, in room-temperature solvent, T_S = 293 K. The results call for a new activation mechanism in the liquid phase.

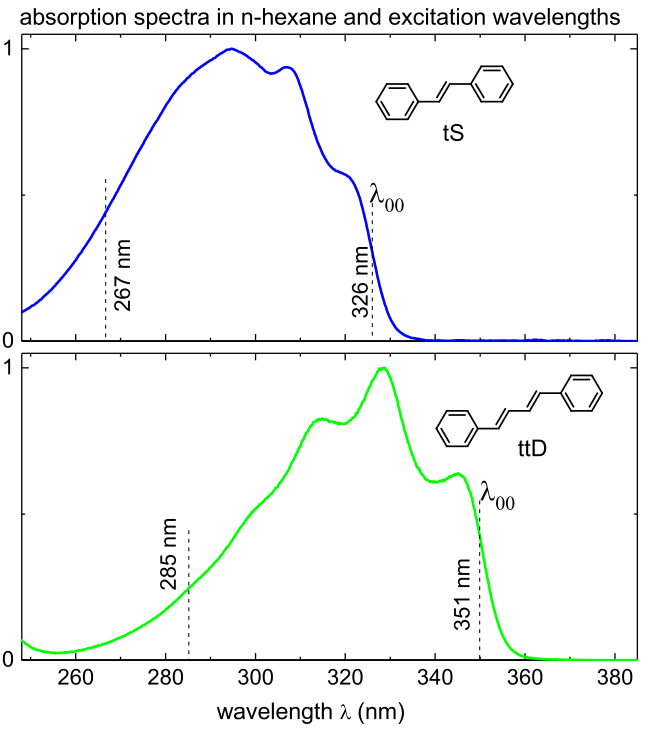

Figure 1. Normalized absorption spectra $A(\lambda)$ of *trans*-stilbene (tS) and trans−trans-diphenylbutadiene (ttD) in *n*-hexane. 0−0 transition λ_{00} and excitation wavelength λ_{exc} for transient absorption (TA) are indicated.

3.1. Transient Absorption Spectra and Photoisomerization Kinetics. Typical TA spectra and kinetics of tS and ttD in *n*-hexane, upon excitation *without* excess vibrational energy, are displayed in Figure 2. The excitation wavelength λ_{exc} was centered at the 0−0 transition, 326 nm for tS, and 351 nm for ttD. In that case the molecule preserves its ground-state temperature, and the TA spectra are not disturbed by vibrational cooling in the S_1 state.[22] The spectra consist of three well separated bands: bleach, stimulated emission (SE), and excited-state absorption (ESA); bleach and SE are negative, while ESA is positive.

The observed sub-ns decays of ESA and SE mainly correspond to excited-state isomerization $S_1 \rightarrow P$ to perpendicular conformation *P* over a barrier, while subsequent relaxation $P \rightarrow S_0$ is barrier less and ultrafast, of ∼0.1 ps.[24] Other deactivation paths, like direct (vertical) internal conversion[66,67] or intersystem crossing, are much slower than the $S_1 \rightarrow P$ isomerization and can be safely neglected. (For instance, in closely related *trans*-naphtylstilbene the fastest relaxation pathway is radiative, with a lifetime of several ns.[68]) In this picture the bleach recovery develops with the same time constant τ as the decay of ESA. Figures S1 and S2 in Supporting Information confirm that this is indeed the case

https://doi.org/10.1021/jacs.4c09134
J. Am. Chem. Soc. 2024, 146, 32463−32478

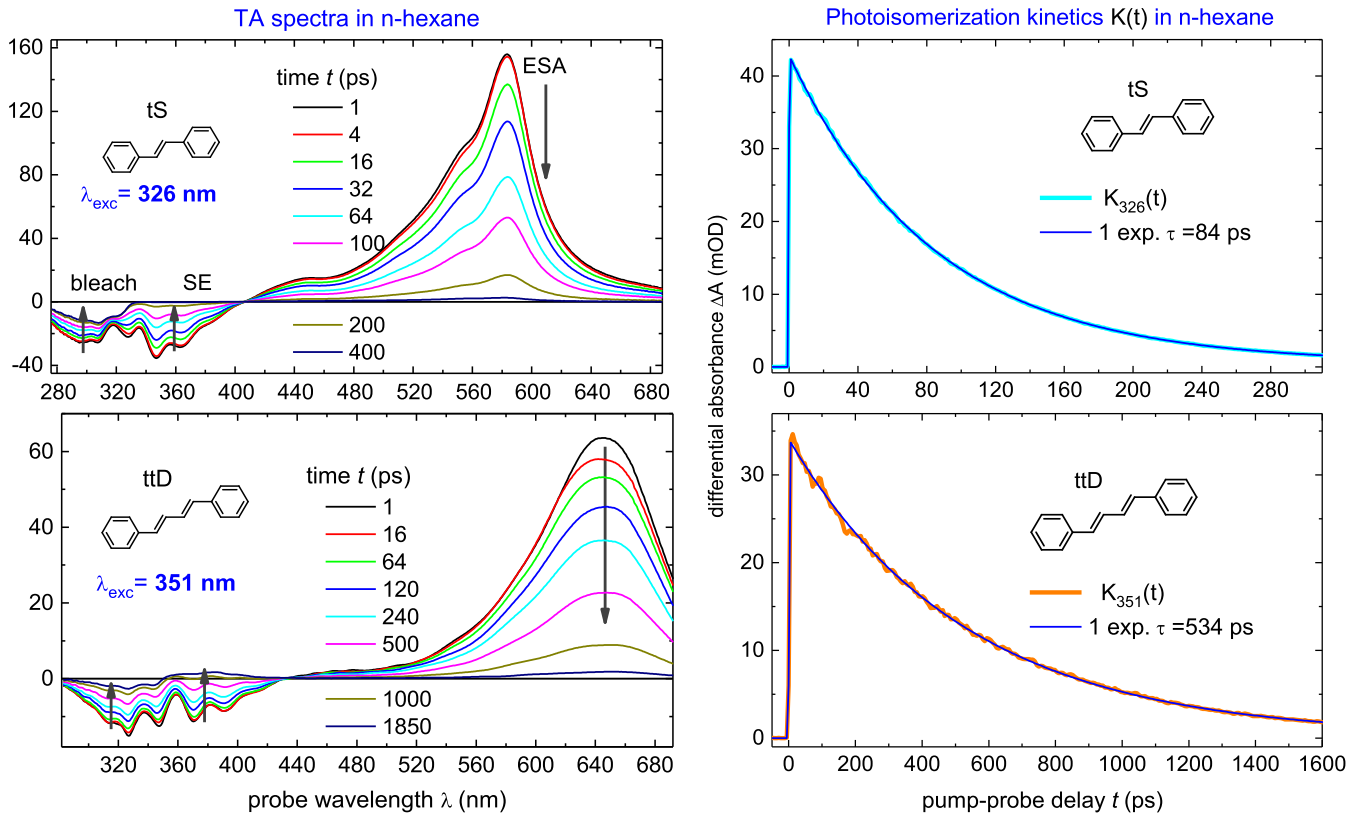

Figure 2. TA spectra upon $S_0 \rightarrow S_1$ excitation *without* excess vibrational energy in *n*-hexane at $T = 20$ °C, $\lambda_{exc} = 326$ nm for tS, and 351 nm for ttD. Bleach and stimulated emission (SE) are negative, excited-state absorption (ESA) is positive. The subns decay of ESA and SE reflect photoisomerization $S_1 \rightarrow P$ over a barrier to perpendicular state *P*, while subsequent relaxation $P \rightarrow S_0$ is barrier less and ultrafast, of ~0.1 ps. At late time, the cis and trans products are seen in the bleach region. Photoisomerization kinetics $K(t)$, eq 5, are derived from the ESA decay, fitted monoexponentially with time τ, thus giving the rate $k_{iso} = 1/\tau_{iso} = (1/\tau - 1/\tau_{rad})$, with $\tau_{rad} = 1.6$ ns for tS, or 1.5 ns for ttD. See Figures S1 and S2 in Supporting Information for more details.

Table 1. Solvent Properties, Rotational Time τ_R, Photoisomerization Time τ_{iso} at Room Temperature[a]

solvent	ε	n	M (g/mol)	D (g/cm^3)	V_m (Å^3)	V_{VdW} (Å^3)	α (Å^3)	η (cP)	τ_R tS (ps)	τ_{iso} tS (ps)	τ_R ttD (ps)	τ_{iso} ttD (ps)
pe C_5H_{12}	1.858	1.357	72.15	0.621	193	96	10.2	0.234	10	80	19	712
ipe C_5H_{12}	1.858	1.357	72.15	0.621	193	96	10.2	0.225			20	661
he C_6H_{14}	1.898	1.375	86.18	0.659	213	113	11.9	0.307	14	89	23	829
hp C_7H_{16}	1.936	1.388	100.2	0.684	245	130	13.8	0.418	17	98	28	938
oc C_8H_{18}	1.965	1.398	114.2	0.699	271	147	15.6	0.547	22	108	35	1051
ioc C_8H_{18}	1.965	1.397	114.2	0.699	271	147	15.6	0.547			36	782
dc $C_{10}H_{22}$	2.005	1.412	142.2	0.726	325	215	19.2	0.925	28	125	58	1214
hd $C_{16}H_{34}$	2.057	1.435	226.4	0.77	488	283	30.3	3.125	78	178	170	1843
ch C_6H_{12}	2.038	1.426	84.16	0.774	181	102	11.0	0.977	35	83	60	1037
pfh C_6F_{14}	1.582	1.248	338.0	1.691	333	137	12.7	0.708	21	53		
db $C_8H_{18}O$	3.172	1.399	130.2	0.764	283	153	16.3	0.689	27	85	50	489
de $C_4H_{10}O$	4.305	1.352	74.12	0.708	174	86	8.98	0.254	13	63	23	147
th C_4H_8O	7.729	1.407	72.11	0.884	136	72	7.97	0.53	24	74	41	125
ac C_2H_3N	36.69	1.344	41.05	0.776	88	47	4.44	0.357	17	41	31	26
me CH_4O	33.65	1.328	32.04	0.791	68	36	3.3	0.587			49	36

[a]21 °C for tS, 20 °C for ttD. Solvents: *n*-pentane (pe), isopentane (ipe), *n*-hexane (he), *n*-octane (oc), isooctane (ioc), *n*-decane (dc), *n*-hexadecane (hd), cyclohexane (ch), *n*-perfluorohexane (pfh), *n*-dibutylether (db), *n*-diethyl ether (de), tetrahydrofuran (th), acetonitrile (ac), methanol (me). ε, n dielectric constant and refractive index, $V_m = M/DN_A$ solvent volume per molecule, V_{VdW} molecular van der Waals volume, α polarizability, N_A Avogadro number.

both for tS and ttD. The bleach signal at late time in Figure 2 corresponds to newly created cis and trans products in S_0. The photoisomerization dynamics of tS and ttD and of their cis isomers has been studied and analyzed in detail in our previous publications.[24−28,41,53]

The photoisomerization kinetics $K(t)$ are given by a band integral

$$K(t) = \frac{1}{\ln(\lambda_2/\lambda_1)} \int_{\lambda_1}^{\lambda_2} \Delta A(\lambda, t) \mathrm{d}\lambda/\lambda \quad (5)$$

https://doi.org/10.1021/jacs.4c09134
J. Am. Chem. Soc. 2024, 146, 32463−32478

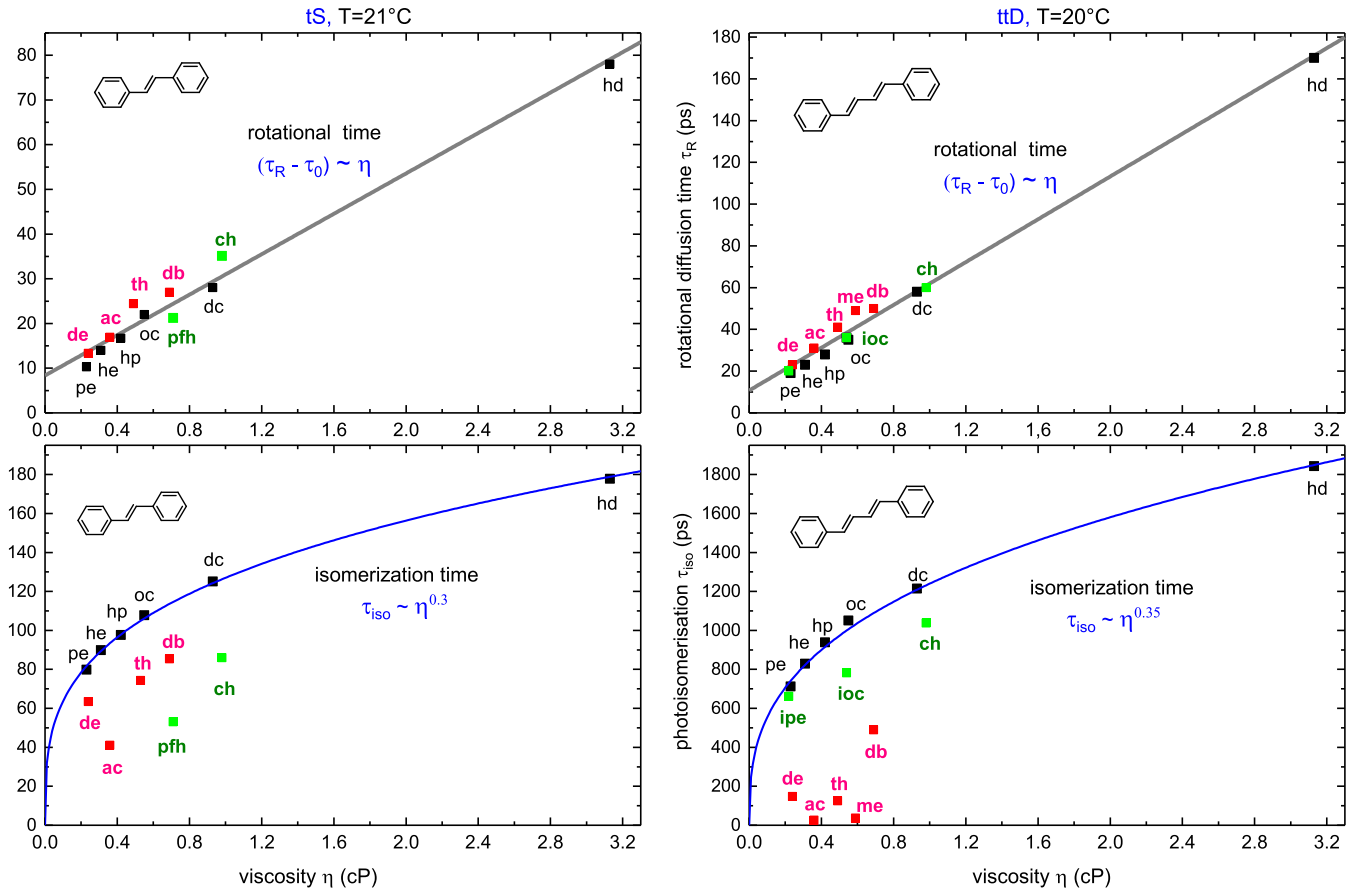

Figure 3. Rotational time τ_R (top) and photoisomerization time τ_{iso} (bottom) as a function of solvent viscosity η at 20 °C for tS and 21 °C for ttD. The solvents are listed in Table 1. Note the linear dependence $(\tau_R - \tau_0) \sim \eta$ with $\tau_0 = \tau_R(0)$, and the power dependence $\tau_{iso} \sim \eta^{\alpha}$ for *n*-alkanes (in black), with $\alpha = 0.30$ for tS, or $\alpha = 0.35$ for ttD. Large deviations from the fit for pfh, ch, ioc (in green) possibly indicate molecular size effects, while the deviations in polar solvents (in red) come from lowering the $S_1 \rightarrow P$ barrier due to polar *P*-state.

where the integration is over the ESA region, 450−680 nm for tS, and 540−690 nm for ttD. In case of a monoexponential decay kinetics with time τ, the photoisomerization rate k_{iso} is obtained as

$$k_{iso} = 1/\tau_{iso} = (1/\tau - 1/\tau_{rad}) \quad (6)$$

where τ is the fitted decay time, and τ_{rad} is the radiative time, 1.6 ns for tS,[24] or 1.5 ns for ttD in solution.[38]

3.2. Viscosity Dependence of the Reaction Rate at Room Temperature. We measured isomerization time τ_{iso} and rotational time τ_R of tS and ttD for a broad selection of solvents. The results are summarized in Table 1 and depicted in Figure 3. The solvents include *n*-alkanes (black symbols), isoalkanes, (green), perfluorohexane and cyclohexane (also in green), and polar solvents (red).

The rotational time τ_R depends linearly on viscosity η

$$(\tau_R - \tau_0) \sim \eta \quad (7)$$

where $\tau_0 = \tau_R(0)$ is obtained from a linear fit at $\eta = 0$. This gives for tS $\tau_0 = 8$ ps, and for ttD $\tau_0 = 10$ ps, that is close to free molecular rotation time $2\pi\sqrt{I_m/kT} = 15$ ps at 293 K where I_m is the moment of inertia of tS or ttD. Note, the fit includes all the solvents measured, that is, τ_R depends linearly on viscosity η and is not affected by other solvent properties.

Next, the photoisomerization times τ_{iso} are shown in lower panel of Figure 3. Here a good fit is possible through *n*-alkanes

$$\tau_{iso} \sim \eta^{\alpha} \quad (8)$$

with $\alpha = 0.30$ for tS, and $\alpha = 0.35$ for ttD.

The dependence (8) was reported previously by many authors.[12,13,16,17,29,30,33] Deviations from the fit in polar solvents are due to the polar *P*-state that lowers the isomerization barrier E_b.[27−29,41] This results in decreasing τ_{iso} in solvents of higher polarity from dibutylether to acetonitrile, both for tS and for ttD. The stabilization is stronger for ttD, in agreement with its more polar *P* state.[41] Note also strong deviations from the fit (8) in nonpolar isoalkanes, cyclohexane and perfluorohexane, which are possibly due to molecular size effects. We return to this point in Section 4.4.

3.3. Temperature-Dependent Isomerization Rate and Rotational Rate. We simultaneously measure in the same pump−probe scan the rotational time τ_R and the photoisomerization time τ_{iso} at solvent temperature T_S = 10, 20, 30, 40, 50 °C. The results are collected in Tables 2−5 and displayed in Figure 4. The figure shows that the dependencies (7) and (8) are reproduced with the same fit parameters for all temperatures T_S.

Figure 5 shows Arrhenius fits of photoisomerization rate $k_{iso} = 1/\tau_{iso}$ and of modified rotational rate $1/(\tau_R - \tau_0)$. A good linear dependence confirms the Arrhenius behavior of the rates, $k_{iso} = A\exp(-E_b/kT)$ and $1/(\tau_R - \tau_0) \sim \exp(-E_\eta/kT)$. Note, the barrier E_b includes both the viscosity contribution αE_η and the intramolecular barrier E_{in}. The slope **b**, as indicated in the insets of Figure 5, provides isomerization/

https://doi.org/10.1021/jacs.4c09134
J. Am. Chem. Soc. 2024, 146, 32463−32478

Table 2. tS Photoisomerization Time τ_{iso} (ps)[a]

T_S (K)	he	hp	oc	dc	hd	ch	ac	D2 ac
283	120	130	146	170		110	51	70
293	89	97	108	125	178	86	40	55
303	69	76	84	95	130	74	33	44
313	56	60	68	76.5	95	60	28	36
323	45	52	55	63	73	50	23	

[a]D2 − tS deuterated at the ethylenic bond.

Table 3. tS Rotational Time τ_R (ps)

T_S (K)	he	hp	oc	dc	hd	ch	ac	D2 ac
283	17	21	26	40	46	22	21	21
293	14	17	22	28	38	17	18	17
303	12	16	18	26	28	15	15	15
313	11	12	16	23	22	13	14	14
323	10	11	14	20	20	11	11	

Table 4. ttD Photoisomerization Time τ_{iso} (ps)

T_S (K)	he	hp	oc	dc	hd	ch
293	830	935	1071	1214	1843	1034
303	599	697	782	917	1204	715
313	430	507	562	639	832	531
323	331	369	436	507	682	391

Table 5. ttD Rotational Time τ_R (ps)

T_S (K)	he	hp	oc	dc	hd	ch
293	24	28	36	57	170	62
303	23	25	33	43	111	49
313	19	22	26	38	81	39
323	17	19	22	33	68	33

viscosity barriers $E_{b,\eta} = -R\cdot\mathbf{b}$ (in kJ/mol, R = 8.314 J/K/mol), and the intercept $\mathbf{a}$ gives preexponential factors $A = e^{\mathbf{a}}$. Furthermore, the dependencies $\tau_{iso} \sim \eta^{\alpha}$, $(\tau_R - \tau_0) \sim \eta$ allow for determining the viscosity contribution αE_η to barrier E_b, and deriving the inner (intramolecular) barrier in solution

$$E_{in} = (E_b - \alpha E_\eta) \tag{9}$$

Although the viscosity contribution αE_η is obtained for *n*-alkane only, we believe that eq 9 can also be used for polar solvents and branched alkanes, at least as a rough estimate.

The Arrhenius fit parameters are collected in Table 6 for tS, and in Table 7 for ttD. It follows that the intramolecular barrier E_{in} closely matches the gas-phase barrier obtained by Zewail and co-workers[8−11] for tS (Table 6). The barrier difference between the gas phase and alkanes of 160 cm^{-1} may be due to the stabilization of polar P by the dispersive and induction interaction in nonpolar solvents.[69] For ttD, a comparison between the gas and solution reaction rate is not appropriate as the S_1 state switches from 2^1A_g in jet/gas to 1^1B_u in solution. Remarkably, for tS in *n*-alkanes the preexponential factor A is about 10 times larger than in the gas phase. Important consequences from this observation are discussed in Section 3.6.

3.4. Isoviscosity Rate. We consider now the so-called isoviscosity rate[16,17] s originally introduced to eliminate the viscosity dependence in k_{iso} and get thus the intramolecular barrier E_{in}. We obtain these rates by fitting $\tau_{iso}(\eta)$ in *n*-alkanes in the range $0.2 < \eta < 1.1$ cP as illustrated in Figure 6 (left). We then get isoviscosity times τ_i from the fits at a given viscosity and temperature. Arrhenius fits of such obtained isoviscosity rates (for η = 0, 0.25, 0.5, 1 cP) are shown in Figure 6 (right), where the slope $\mathbf{b}$ tends to *increase* with decreasing η. In other words, the intramolecular barrier E_{in} appears to become higher by lowering η, which seems unphysical. We therefore rely on our estimate of the viscosity contribution αE_η to E_b (Section 3.3) in order to derive the intramolecular barrier E_{in} in solution.

3.5. Excitation Wavelength Dependence in Jet/Gas. Our analysis of the gas-phase photoisomerization is largely based on results by Zewail and co-workers.[11] They measured the photoisomerization of tS at collisionless conditions with λ_{exc} = 306, 294, 285, 280, 277 nm, and derived both IVR rates k_{IVR} and reaction rates k_{iso}. Their isomerization kinetics, reproduced in Figure 7 at left, reveal a strong dependence on λ_{exc}. Here the magenta curve with λ_{exc} = 265 nm is by Hochstrasser and co-workers.[5] The jet/gas kinetics shall be compared to the kinetics in solution in Section 3.6.

The IVR rate was determined to be faster than 1 ps^{-1}.[11] As the shortest isomerization time is 15 ps, this suggests that the IVR is complete in jet/gas, and molecular temperature T_m can be calculated from the energy distribution over molecular vibrational modes ν_j

$$E_{th} + (1/\lambda_{exc} - 1/\lambda_{00}) = \sum_j \nu_j/[(\exp(\nu_j/kT_m) - 1)] \tag{10}$$

where E_{th} = 1870 cm^{-1} is molecular thermal vibrational energy at 294 K, and λ_{00} = 310 nm is the 0−0 transition for tS in jet/gas. Vibrational frequencies ν_j in S_1 are obtained by quantum chemical computations (see Supporting Information), and the isomerization rate $k_{iso} = (1/\tau - 1/\tau_{rad})$ is calculated with τ_{rad} = 3.2 ns in gas.[9]

An Arrhenius fit to eq 1 of k_{iso} is shown in Figure 7 at right. The linear fit is of good quality and results in ν_{iso} = (60 ± 5) cm^{-1}, $E_b = E_{in}$ = (1398 ± 26) cm^{-1}, with a preexponential factor $A_m = c\nu_{iso}$ = (1.81 ± 0.16) ps^{-1}. Thus, the jet/gas data[5,11] agree with the RRKM eq 1 and deliver the key quantities E_{in} and ν_{iso}.

3.6. Excitation Wavelength Dependence in Solution. We now turn to the photoisomerization in solution, recorded at zero and high excess vibrational energy, Figure 8. The photoisomerization kinetics $K_\lambda(t)$ are calculated with eq 5, the subscript indicates λ_{exc}. For tS the ESA range 450−680 nm can still be used in eq 5, as the ESA band is completely within the registration window; its blue shift and narrowing in the course of vibrational cooling does not affect the band integral. For ttD, however, the ESA band extends beyond the registration range, and the spectral shift and band narrowing may change the integral. Therefore, the bleach region 300−350 nm is chosen to calculate $K_\lambda(t)$ for ttD.

As seen from Figure 8, the decay in solution is nearly insensitive to λ_{exc}, unlike in jet/gas at collisionless conditions, Figure 7. With zero excess vibrational energy ($\lambda_{exc} = \lambda_{00}$) the kinetics is monoexponential, τ = 84 ps for tS in *n*-hexane, and τ = 26.3 ps for ttD in acetonitrile. For high excess energy, λ_{exc} = 267 nm for tS, or λ_{exc} = 285 nm for ttD, the behavior (cyan curve) is quite similar, differing by a small extra-decay at early time. A biexponential fit $K_\lambda(t) = [a_1 \exp(-t/\tau_1) + a_2 \exp(-t/\tau_2)]$ gives for tS in *n*-hexane τ_1 = 10 ps, a_1 = 0.06, τ_2 = 84 ps, and for ttD in acetonitrile τ_1 = 10 ps, a_1 = 0.10, τ_2 = 26 ps.

https://doi.org/10.1021/jacs.4c09134
J. Am. Chem. Soc. 2024, 146, 32463−32478

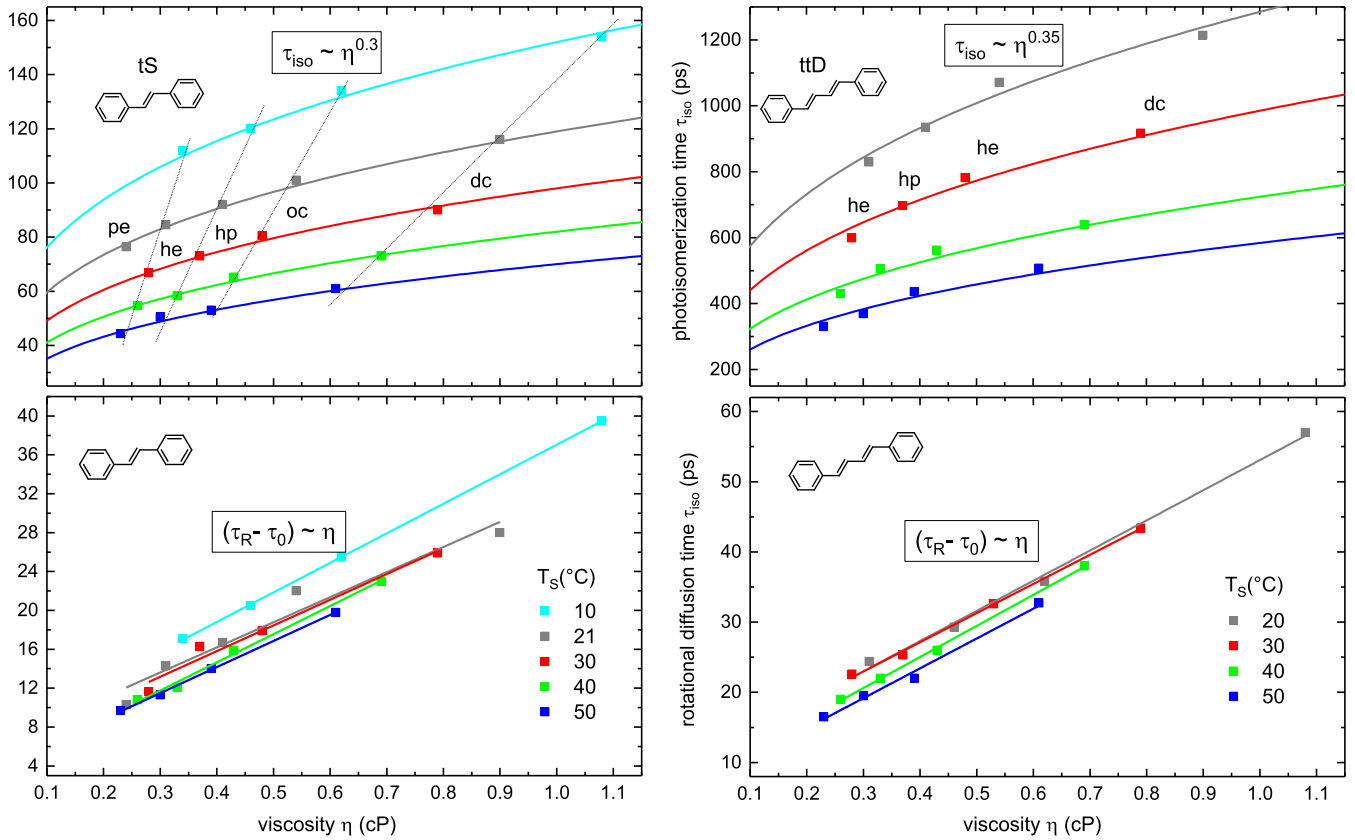

Figure 4. Photoisomerization time $\tau_{iso} \sim \eta^{\alpha}$ (top) is fitted with $\alpha = 0.30$ for tS, and $\alpha = 0.35$ for ttD, for temperatures $T_S = 10$, 20, 30, 40, 50 °C. Rotational time τ_R (bottom) is fitted linearly $(\tau_R - \tau_0) \sim \eta$ with $\tau_0 = \tau_R(0)$.

We have to check now if the kinetics, recorded at high excess vibrational energy, can be reproduced by k_{RRKM}, eq 1, with nonstationary molecular temperature[20,22]

$$T_m(t) = T_S + (T_0 - T_S)\exp(-t/\tau_c) \tag{11}$$

Here $T_0 = 607$ K is the initial temperature of tS for $\lambda_{exc} = 267$ nm obtained from eq 10, $T_S = 294$ K is solvent temperature, and $\tau_c \approx 10$ ps is the molecular cooling time in solution. It was shown[22] that eq 11 works well in aprotic solvents like *n*-hexane or acetonitrile. The kinetics $K_\lambda(t)$ can then be recast as

$$\ln K_\lambda(t) = -\int_0^t dt[1/\tau_{rad} + A_m \exp(-E_b/kT_m(t))] \tag{12}$$

where $A_m = 19.4$ ps^{-1}, $E_b = 1520$ cm^{-1} should be taken from Table 6.

Figure 9 compares experimental kinetic K_{267} for tS to the RRKM simulations by eq 12. Clearly, k_{RRKM} cannot fit the experimental curve with any cooling time in the range $0.3 < \tau_c < 10$ ps (top panel). Even for unreasonably short $\tau_c = 0.3$ ps, the early decay cannot be reproduced. Alternatively, with $A_m = 0.7$ ps^{-1} one may fit the very early behavior but then the late decay substantially deviates (middle panel).

Nonetheless, we have shown in Section 3.5 that eq 1 is correct for isolated tS in jet/gas (Figure 7). Hence, k_{RRKM} should also contribute to the rate in solution. Indeed, the photoisomerization kinetics is biexponential, $K_{267} = [a_1 \exp(-t/\tau_1) + a_2 \exp(-t/\tau_2)]$ where the fast component $\tau_1 \approx \tau_c$ reflects the cooling of tS molecule. It is therefore natural to ascribe the fast decay to the intramolecularly activated tS isomerization (molecular contribution). The slower component should then represent the solvent-induced isomerization, as activated by solute−solvent collisions. The interpretation is supported by the results in buffer gases[14,18] where the rate k_{iso} is proportional to the buffer pressure, or to the collision rate of tS and buffer molecules. At high molecular temperature T_m, the intramolecular activation dominates because of a high exponential factor, while at $T_m = T_S$ the solvent activation prevails due to a large frequency of solute−solvent collisions. Thus, the photoisomerization rate in solution can be expressed as[27]

$$k_{iso}(t) = A_m \exp(-E_b/kT_m(t)) + A_S \exp(-E_b/kT_S) \tag{13}$$

Here the first term is the intramolecular part, with temperature $T_m(t)$ from eq 11. For tS we expect $A_m \sim 1$ ps^{-1} similar as in jet (Figure 7). The second term is the solvent contribution at temperature T_S, induced by solute−solvent collisions, A_S being the collision rate. Notice, T_m and T_S in eq 13 are generally *different* as the probe molecule is heated up upon ultrafast optical excitation. When $\lambda_{exc} = \lambda_{00}$ no heating occurs, $T_m = T_S$ and eq 13 reads

$$k_{iso} = (A_m + A_S)\exp(-E_b/kT_S) = A \exp(-E_b/kT_S) \tag{13a}$$

The rate has the same form as eq 1 with $A = (A_m + A_S)$. Taking $A = 19.4$ ps^{-1} in *n*-hexane and $A_m = 1.8$ ps^{-1} from Table 6 one gets $A_S = 17.6$ ps^{-1}. Thus, at room temperature the solvent contribution to the photoisomerization rate is 10 times higher than the intramolecular contribution.

A reasonable fit to eq 13 is obtained with $A_m = 0.7$ ps^{-1}, $A_S = 18$ ps^{-1}, $E_b = 1520$ cm^{-1}, $\tau_c = 10$ ps, $T_0 = 607$ K, $T_S = 294$ K, as shown in low panel of Figure 9. The fit is good, indicating the

https://doi.org/10.1021/jacs.4c09134
J. Am. Chem. Soc. 2024, 146, 32463−32478

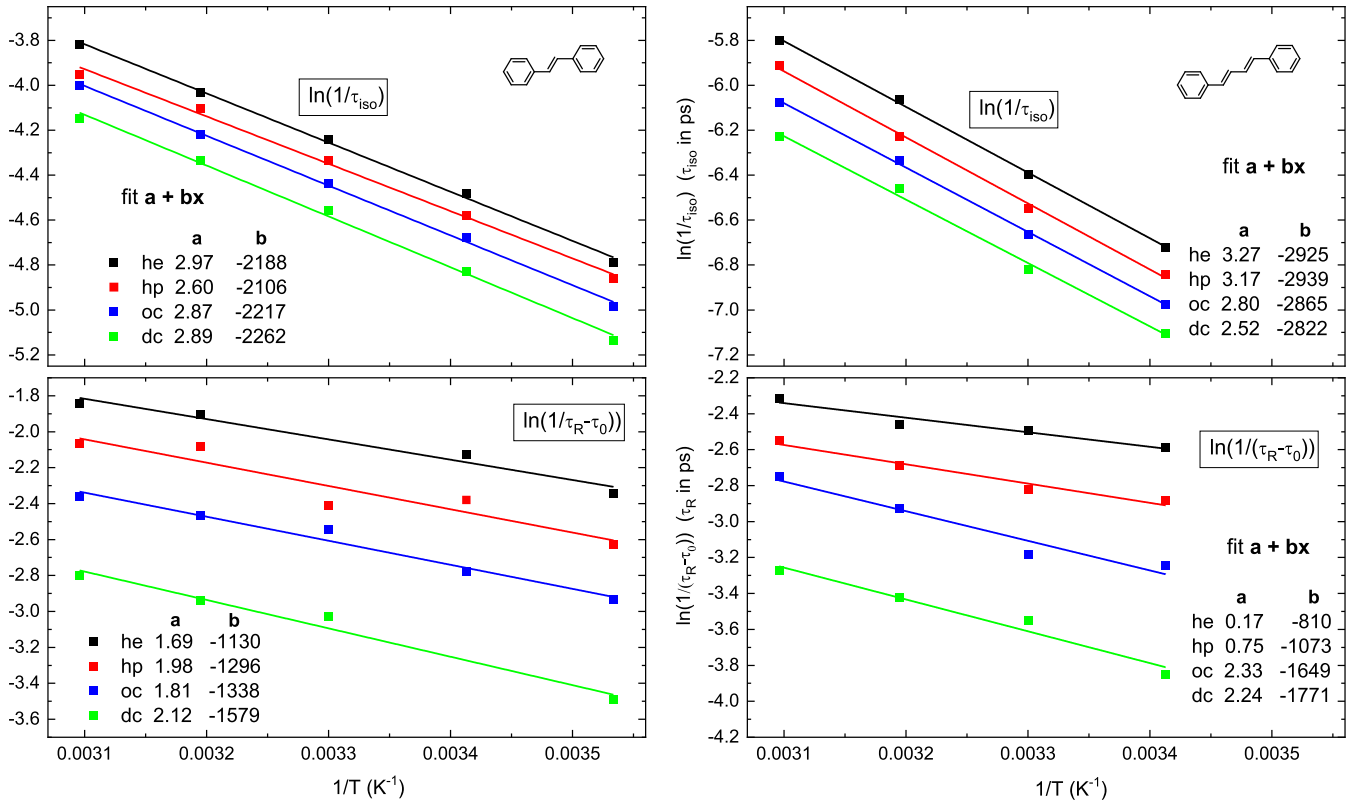

Figure 5. Arrhenius fits of photoisomerization rate $k_{iso} = 1/\tau_{iso} = A\exp(-E_b/kT_S)$ and of modified rotational rate $k_R = 1/(\tau_R - \tau_0) \sim \exp(-E_\eta/kT_S)$, T_S = 10, 20, 30, 40, 50 °C. Slopes **b** give isomerization/rotation barriers $E_{b,\eta} = -R\cdot\mathbf{b}$ in kJ/mol, R = 8.314 J/K/mol, and intercept **a** gives preexponential factor $A = e^a$. From $\tau_{iso} \sim \eta^\alpha$ and $(\tau_R - \tau_0) \sim \eta$ one gets the inner barrier $E_{in} = (E_b - \alpha E_\eta)$ in solution.

Table 6. tS, Arrhenius Fit Parameters[a,b]

	η (cP)	A (ps^{-1})	E_b (cm^{-1})	E_η (cm^{-1})	E_{in} (cm^{-1})
ac	0.36	13.1	1277	920	1001
he	0.307	19.4	1520	904	1249
hp	0.418	13.5	1464	961	1176
oc	0.547	17.6	1541	970	1250
dc	0.925	17.9	1572	1009	1269
mean over alkanes					1236 ± 36
jet/gas[11]		1.8[b] ± 0.2			1398[b] ± 26
jet/gas[19]		0.74			1155

[a]$E_{in} = (E_b - 0.30\cdot E_\eta)$. [b]This work.

Table 7. ttD, Arrhenius Fit Parameters[a]

	η (cP)	A (ps^{-1})	E_b (cm^{-1})	E_η (cm^{-1})	E_{in} (cm^{-1})
he	0.307	26	2033	563	1836
hp	0.418	24	2043	746	1782
oc	0.547	16	1991	1146	1590
dc	0.925	12	1961	1231	1530
mean					1680 ± 130
jet/gas[19,32]		0.86			1000

[a]$E_{in} = (E_b - 0.35\cdot E_\eta)$.

model captures main features of the photoisomerization in solution. Note that the fitted value A_m = 0.7 ps^{-1} in *n*-hexane corresponds to the reactive mode ν_{iso} = 23 cm^{-1} that is substantially smaller than ν_{iso} = 60 cm^{-1} measured in jet (Figure 7), indicating that the effective isomerization path/frequency in solution is different from that in the isolated molecule.

To sum up this section, eq 13 suggests a new expression for photoisomerization rate in solution, where the reaction is concomitant to vibrational cooling. In jet/gas at collisionless conditions, the molecule is at constant temperature T_m and isomerizes with constant rate k_{RRKM} of eq 1, determined by excess energy $(1/\lambda_{exc} - 1/\lambda_{00})$. In solution, $T_m(t)$ decreases to solvent temperature T_S, eq 11, the intramolecularly activated isomerization slows down to reveal a new isomerization mechanism, due to activation by solute−solvent collisions. The latter is 10 times more efficient than the intramolecular activation. A possible mechanism behind the collisional activation is that the phenyl rings of tS or ttD upon colliding with solvent molecules acquire a momentum perpendicular to the molecular plane that promotes isomerization about the ethylenic bond.

3.7. Deuteration Effect on the Isomerization Rate.

Further interesting and corroborating results are obtained with deuterated stilbenes D2, D10, D12 (with ethylenic, phenyl, and full deuteration, respectively, while D0 means no deuteration). Figure 10 displays photoisomerization kinetics K_{326} in *n*-hexane and acetonitrile, $\lambda_{exc} = \lambda_{00}$ = 326 nm. It is seen that the kinetics is indistinguishable for D0, D10, and for D2, D12. Next, the D2 rate is 1.4-fold slower than that of D0. How can this be explained in view of eq 13?

The solvent contribution A_S to the rate k_{iso} is proportional to the frequency of solute−solvent collisions that depends on the area of phenyl rings and solvent properties. The effect of increased mass on the momentum of the phenyl rings is rather modest even in D12, while in D2 the rings are not affected at all. Therefore, we expect A_S to be roughly the same for all the

https://doi.org/10.1021/jacs.4c09134
J. Am. Chem. Soc. 2024, 146, 32463−32478

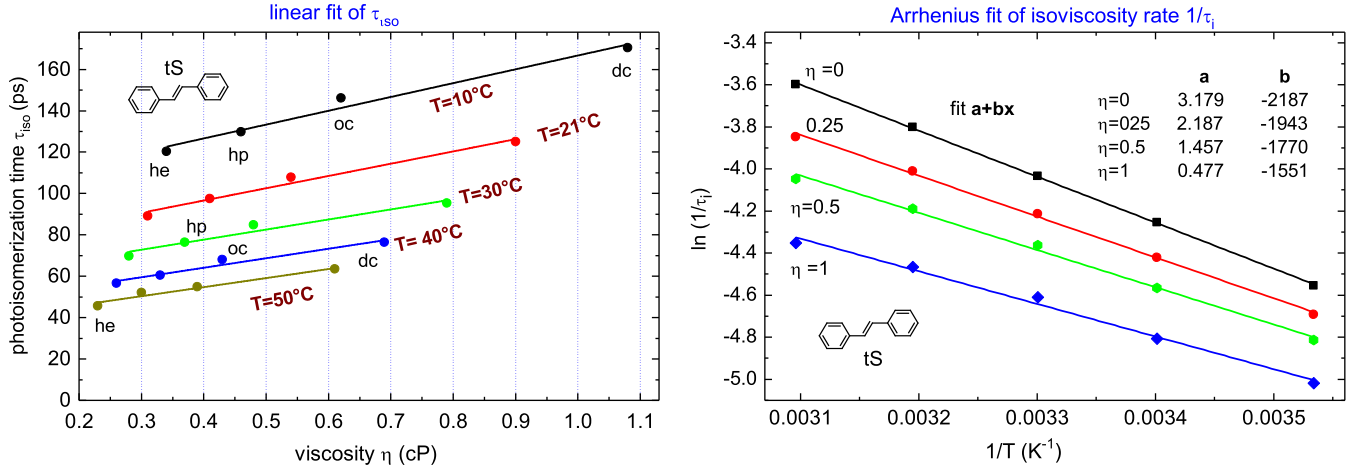

Figure 6. Linear fits of τ_{iso} for *n*-alkanes (left) allow for isoviscosity times τ_i at given viscosity η (right). Arrhenius fits of isoviscosity rates $k_i = 1/\tau_i = A\ \exp(-E_i/kT_S)$ result in *higher* barriers E_i for lower η, leading to unphysical results.

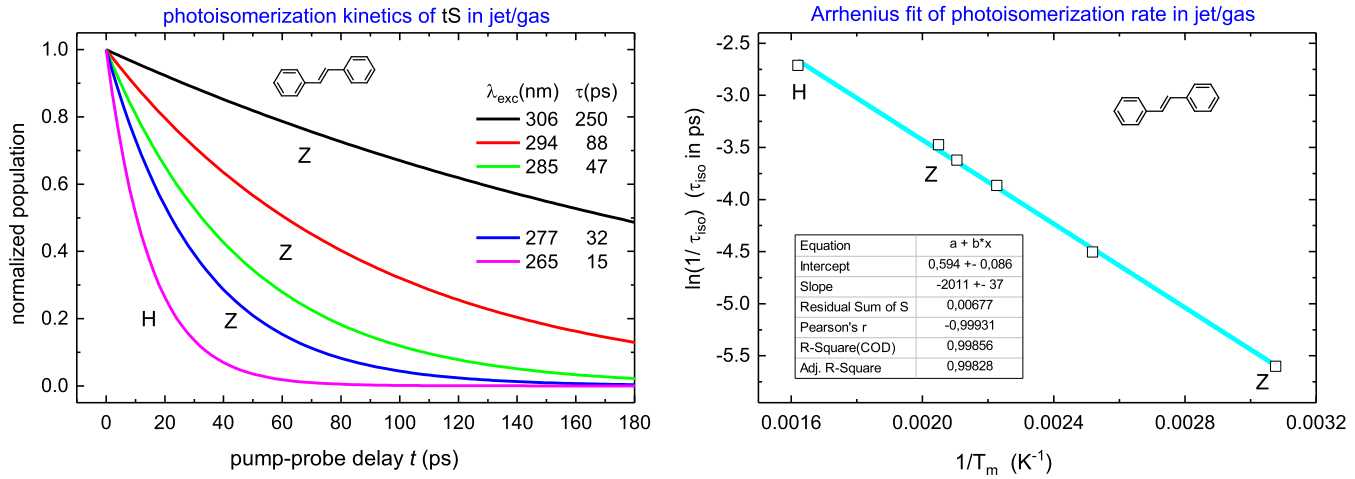

Figure 7. Photoisomerization kinetics of tS in jet/gas (at left) from Zewail (Z, ref 11.) and Hochstrasser (H, ref 5.) with different λ_{exc}. The decay time τ strongly depends on λ_{exc} and shortens from 250 ps (306 nm) to 15 ps (265 nm), giving the isomerization rate $k_{iso} = 1/\tau_{iso} = (1/\tau - 1/\tau_{rad})$ with τ_{rad} = 3.2 ns. An Arrhenius fit to $k_{RRKM} = A_m \exp(-E_{in}/kT_m)$ results in E_{in} = (1398 ± 26) cm^{-1}, A_m = (1.81 ± 0.16) ps^{-1} or ν_{iso} = (60 ± 5) cm^{-1} (at right). Molecular temperature T_m is calculated by eq 10, E_{th} = 1870 cm^{-1} at 294 K (Z), or E_{th} = 3497 cm^{-1} at 390 K (H).

isotopomers. Hence, the rate difference of D0 and D2 (and D10, D12) should originate from the difference in barrier E_b.

We have checked this prediction by measuring temperature-dependent rate k_{iso} for D0 and D2 in acetonitrile at strictly identical conditions. The result is presented in Figure 11, A = (13.0 ± 1.4) ps^{-1}, E_b = (1278 ± 23) cm^{-1} for D0, and A = (13.6 ± 1.3) ps^{-1}, E_b = (1349 ± 19) cm^{-1} for D2. This confirms the equality in preexponential factor A, and the difference in barrier E_b due to the isotope effect on the zero-point energy correction, in agreement with our earlier estimates.[53] The said barrier difference of 71 cm^{-1} in acetonitrile agrees well with that of 67 cm^{-1} reported by Saltiel[70] for D0, D2 in *n*-hexane.

3.8. Two Excited States in ttD. In the gas-phase, the S_1 state of ttD is 2^1A_g with a significant contribution of the double HOMO−LUMO excitation while the S_2 state is essentially singly HOMO−LUMO excited 1^1B_u.[39,40] Despite the loss of symmetry upon twisting, we will, for brevity, extend those designations over twisted geometries when referring to the states characterized by the respective electronic contributions. The available experimental gas-phase estimate of the isomerization barrier from 2^1A_g is ca. 1050 cm^{-1},[32] roughly coinciding with the gas-phase separation between 2^1A_g and 1^1B_u.[40] But in solution the two states reorder, and already in hexane ^1B_u is found about 1200 cm^{-1} below ^1A_g.[38,41] In *n*-hexane, the apparent isomerization barrier increases to E_b = 1750−2150 cm^{-1},[29,41] somewhat below the sum of the gas-phase barrier from 2^1A_g and the above solution-phase separation between 2^1A_g and ^1B_u. Hence two alternative possibilities can be considered: either the solution-phase isomerization barrier is fully due to 1^1B_u, or the solvent field makes 2^1A_g barrierless, and the barrier may then be determined by an interplay of the two states. Since the both states are nonpolar in the Franck−Condon region,[41] the solvent field may cause a decrease in the barrier height, similarly to the case of tS. Indeed, the experiment reveals much faster photoisomerization kinetics for ttD in polar solvents.[41]

Previously, the experimental barrier E_b for ttD was fairly well reproduced at the linear response TDDFT level (where 2^1A_g is effectively missing, and 1^1B_u thus remains uncontested as S_1).[41] The present gas-phase XMCQDPT2 results on 1^1B_u as S_2 agree well with those TDDFT findings. The barrier is observed at a twisting angle of 108° (vs 120° at the TDDFT level) where 1^1B_u closely approaches 2^1A_g and they start to interact.

https://doi.org/10.1021/jacs.4c09134
J. Am. Chem. Soc. 2024, 146, 32463−32478

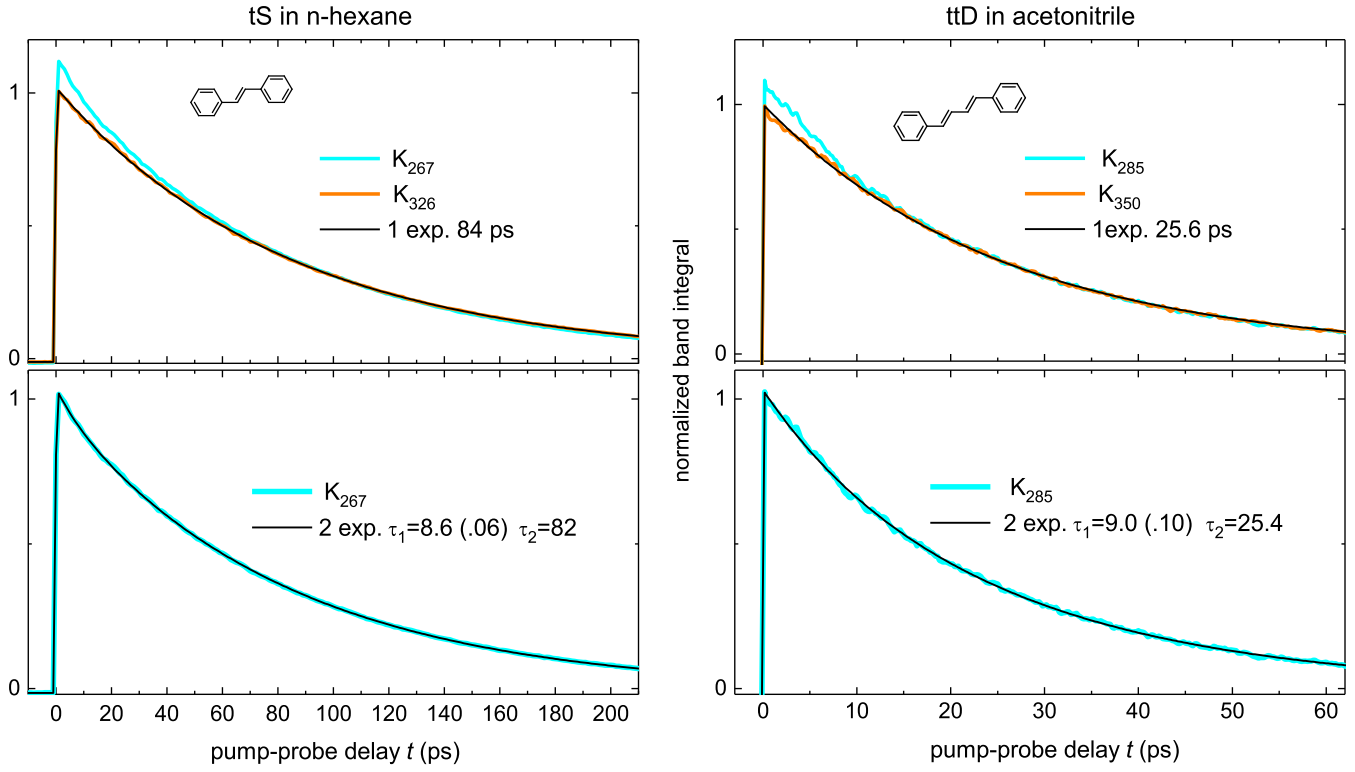

Figure 8. Photoisomerization kinetics $K_\lambda(t)$ where the subscript indicates different λ_{exc}. When $\lambda_{exc} = \lambda_{00}$ (orange) the molecule has no excess vibrational energy, the decay is monoexponential, $\tau = 84$ ps for tS in *n*-hexane, or $\tau = 26.3$ ps for ttD in acetonitrile. At high excess energy (cyan), $\lambda_{exc} = 267$ nm for tS, or 285 nm for ttD, the molecule is initially hot, $T_m(0) \sim 600$ K, and then cools down to solvent temperature $T_S = 293$ K with time $\tau_c \sim 10$ ps. In that case the decay is biexponential, $[a_1 \exp(-t/\tau_1) + a_2 \exp(-t/\tau_2)]$, the fast component a_1 reflects the isomerization activated by hot intramolecular vibrational modes, and the slower component a_2 reflects the isomerization with solvent collisional activation at temperature T_S, eq 13.

In the barrier region, 1^1B_u is only slightly polar, with a dipole moment of 1.9 D. The calculated barrier $E_b = 2650$ cm^{-1} with respect to the origin of 1^1B_u is slightly higher than the TDDFT value, but as a gas-phase estimate, not accounting for the *P*-state stabilization and the barrier lowering in solution, it is still consistent with experiment.[41] Note that the gas-phase origin of 1^1B_u can be established only with symmetry restrictions due to vibronic coupling with 2^1A_g.[32] Previously, we have observed a true, though very shallow, minimum in 1^1B_u at the same XMCQDPT2 level of theory, but such fine details turn out to be highly susceptible to the choice of the model space size.[41]

In 2^1A_g we observe the isomerization barrier at a twisting angle of ca. 91°. Here, the twisting is accompanied by gradually increasing prebarrier polarization associated with pyramidalization of the carbon site next to the phenyl ring. At the transition state, the dipole moment already reaches 7.6 D. Thus, 2^1A_g can, indeed, become barrierless in solution, and may be hence involved in determining the excited-state isomerization barrier E_b. The XMCQDPT2 gas-phase isomerization barrier in 2^1A_g of 2400 cm^{-1} is twice higher than the experimental value.[32] This discrepancy may reflect the limitations of the available computational accuracy, rather than the existence of some alternative isomerization pathway so far unaccounted for.

4. DISCUSSION

4.1. RRKM is Correct in Jet/Gas at Collisionless Conditions. We start with the photoisomerization of tS in jet/gas, as shown in Figure 7. A key result here is that the RRKM rate k_{RRKM} is consistent with the experimental rate $k_{iso} = A_m \exp(-E_b/kT_m)$ at collisionless conditions, where molecular temperature T_m is calculated from λ_{exc} by eq 10. Since eq 10 is valid at the condition of unrestricted IVR, the observed Arrhenius behavior of k_{iso} implies that IVR is *complete* in jet/gas.[11] This agrees with direct measurements of $k_{IVR} > 1$ ps^{-1} by Zewail and co-workers,[11] and with gas-phase results by Troe and co-workers.[19] The Arrhenius fit to eq 1 is good and results in reaction frequency $\nu_{iso} = (60 \pm 5)$ cm^{-1} and barrier $E_{in} = (1398 \pm 26)$ cm^{-1}.

Note that the reactive mode ν_{iso} in jet/gas was not experimentally determined in the past, but was usually derived from computations.[8,10,17,19,44,47,48] This is because the thermal rate $k_{iso}(T)$ was never applied in previous gas-phase studies. Instead, the workers usually measured and analyzed the microcanonical rate $k_{iso}(E)$[8−15,19] as function of excess energy $E = (1/\lambda_{exc} - 1/\lambda_{00})$

$$k_{iso}(E) = N(E - E_b)/(h\rho(E)) \tag{14}$$

Here $N(E - E_b)$ is the number of vibrational states below energy E in the transition state (except the reactive mode ν_{iso}), $\rho(E)$ is the excited-state density of the reactant. It is well-known that the thermal rate $k_{iso}(T)$ can be obtained from $k_{iso}(E)$ by averaging over the thermal distribution[8,19]

$$k_{iso}(T) = kT \int k_{iso}(E)\exp(-E/kT)\rho(E)\mathrm{d}E$$
$$= c\nu_{iso} \exp(-E_b/kT) \tag{15}$$

The second equality is just k_{RRKM}, eq 1, obtained at condition that the vibrational modes in the transition state are the same

https://doi.org/10.1021/jacs.4c09134
J. Am. Chem. Soc. 2024, 146, 32463−32478

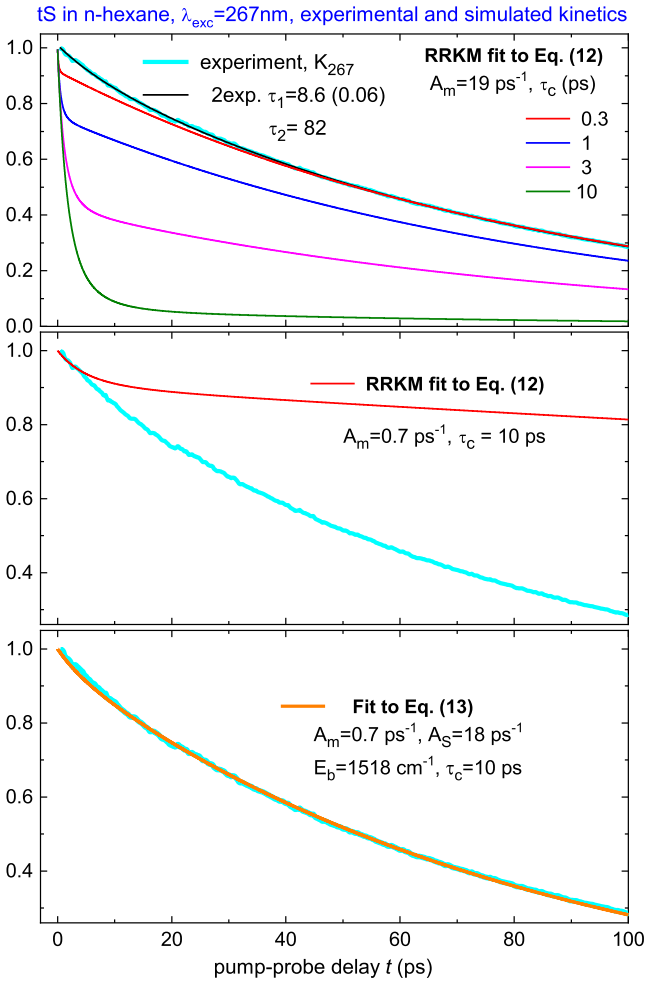

Figure 9. tS photoisomerization kinetics K_{267} (cyan) upon excitation at 267 nm in *n*-hexane, its biexponential fit (black), and simulations to RRKM eq 12, or to eq 13. On top panel are the RRKM simulations with A_m = 19.4 ps^{-1}, E_b = 1520 cm^{-1} (Table 6) and τ_c varying from 0.3 to 10 ps, $T_m(t)$ is from eq 11 with T_0 = 607 K, T_S = 294 K. The simulations for τ_c > 1 ps strongly deviate from experiment, and even for unreasonably short τ_c = 0.3 ps, the early decay cannot be reproduced. The early decay may be reproduced with A_m = 0.7 ps^{-1} ($_m$iddle panel) but then the late behavior deviates considerably. A reasonable fit is possible by eq 13 with A_m = 0.7 ps^{-1}, A_S = 18 ps^{-1} as shown in low panel.

as in the reactant, and $\nu_{iso} \ll kT$. The microcanonical rate $k_{iso}(E)$ is less transparent than $k_{iso}(T)$, furthermore $k_{iso}(E)$ can be evaluated only numerically that in practice requires precalculated ν_{iso}. However, just this rate was commonly applied in the most of gas-phase works.[9−15,17−19] Even Troe and co-workers,[19] who formally considered eq 15, did not derive ν_{iso} and E_{in} from the thermal rate $k_{iso}(T)$. A reason for this was probably historical, as in early stilbene studies there were many uncertain molecular parameters, so the workers preferred to deal with originally measured microcanonical rates $k_{iso}(E)$.

Our analysis of the tS data in jet[11] results in thermal rates $k_{iso}(T)$ that correspond to ν_{iso} = 60 cm^{-1} and $E_b = E_{in}$ = 1398 cm^{-1}. These are different from ν_{iso} = 25 cm^{-1}, E_{in} = 1155 cm^{-1} by Troe and co-workers[19] because their ν_{iso} was taken by hand from the tS vibrational spectrum, while E_{in} was adjusted to fit the experimental rate. In real systems, the approximation of transition state vibrational modes with the reactant modes may be too crude, especially when high-amplitude low-frequency modes are concerned. Thus, the low-frequency twisting modes and the phenyl rotation modes in tS are considerably anharmonic and can actually be coupled, so that $\nu_{iso} = A_m/c$ in eq 13 should be viewed as only an effective parameter.

Also, our intramolecular barrier in nonpolar solution E_{in} = 1236 cm^{-1} is a bit lower than 1398 cm^{-1} in jet, that is probably due to the inductive and dispersive stabilization of the polar *P*-state.[69]

4.2. Two Activation Mechanisms of Isomerization in Solution. The photoisomerization rate dependence on λ_{exc} is weak for tS in solution (Figure 8), in contrast to jet/gas (Figure 7). The main result here is that the behavior at high excess vibrational energy cannot be rationalized in frame of RRKM or Kramers theory, eqs 1 and 2. When one assumes, for example, the validity of eq 1, it is straightforward to simulate photoisomerization kinetics $K_{267}(t)$ at λ_{exc} = 267 nm (see eq 12), with molecular temperature $T_m(t) = T_S + (T_0 - T_S)\exp(-t/\tau_c)$.[22] As seen from Figure 9, the experimental kinetics cannot be reproduced for any conceivable molecular cooling time τ_c in the range 0.3−10 ps.

However, the RRKM rate is correct in jet/gas for the isolated molecule. Therefore, the rate in solution should contain a molecular part. We suggest that this rate is given by the sum of molecular and solvent contribution, eq 13. This model fits well the experimental kinetics K_{267} (Figure 9), reconciles the gas- and solution-phase measurements,[11,18] and further agrees with the results on ttD and deuterated tS (Figures 8, 10, and 11). Note that the collision frequency A_S does not depend on deuteration and should be the same for all the tS isotopomers. This results in identical isomerization kinetics for D0, D10, and for D2, D12 (Figure 10). Moreover, A_S is also of the same value for D0 and D2, while the observed difference in the rate k_{iso} originates from the barrier mismatch of 70 cm^{-1} (Figure 11). The derived barrier mismatch in D0, D2 agrees with a previous estimate by Saltiel et al.[70]

Next, the collision frequency A_S is also identical for ttD and tS by similar arguments. Comparison of Table 6 for tS with Table 7 for ttD shows that the agreement is satisfactory at least in *n*-hexane, *n*-octane, and *n*-decane. Lastly, eq 13 is fully consistent with the linear pressure dependence of k_{iso} in buffer gases.[14,18]

An important observation for ttD is that its lowest S_1 state switches from dark 2^1A_g in jet/gas to bright 1^1B_u in solution.[39−41] That is the photoisomerization occurs in different electronic states, with generally different barrier E_{in} and hence different rate k_{iso}. Thus, for isolated ttD Troe and co-workers[19] obtained the following estimate, $k_{iso}(T)$ = 6.2 ns^{-1} at 20 °C with barrier E_b = 1050 cm^{-1}.[19,32] While the experimental rate in *n*-hexane is k_{iso} = 1.2 ns^{-1} (Table 7). Thus, the reaction is *slower* in solution, because the 1^1B_u barrier E_b = 1836 cm^{-1}, is substantially higher than that in jet/gas.

We believe that a mechanism behind the collisional activation is that solvent collisions with tS or ttD phenyl rings deliver a momentum perpendicular to the molecular plane, thus promoting the ethylenic twist. Another collisional isomerization mechanism was proposed by Hamaguchi and co-worker[21] in frame of their dynamic polarization model. They assumed that solvent collisions with the tS ethylenic bond may directly bring the molecule to the polar *P*-state, and in this way induce the isomerization. This mechanism would be difficult to distinguish from the considered here, as the consequences for the photoisomerization rate are similar.

https://doi.org/10.1021/jacs.4c09134
J. Am. Chem. Soc. 2024, 146, 32463−32478

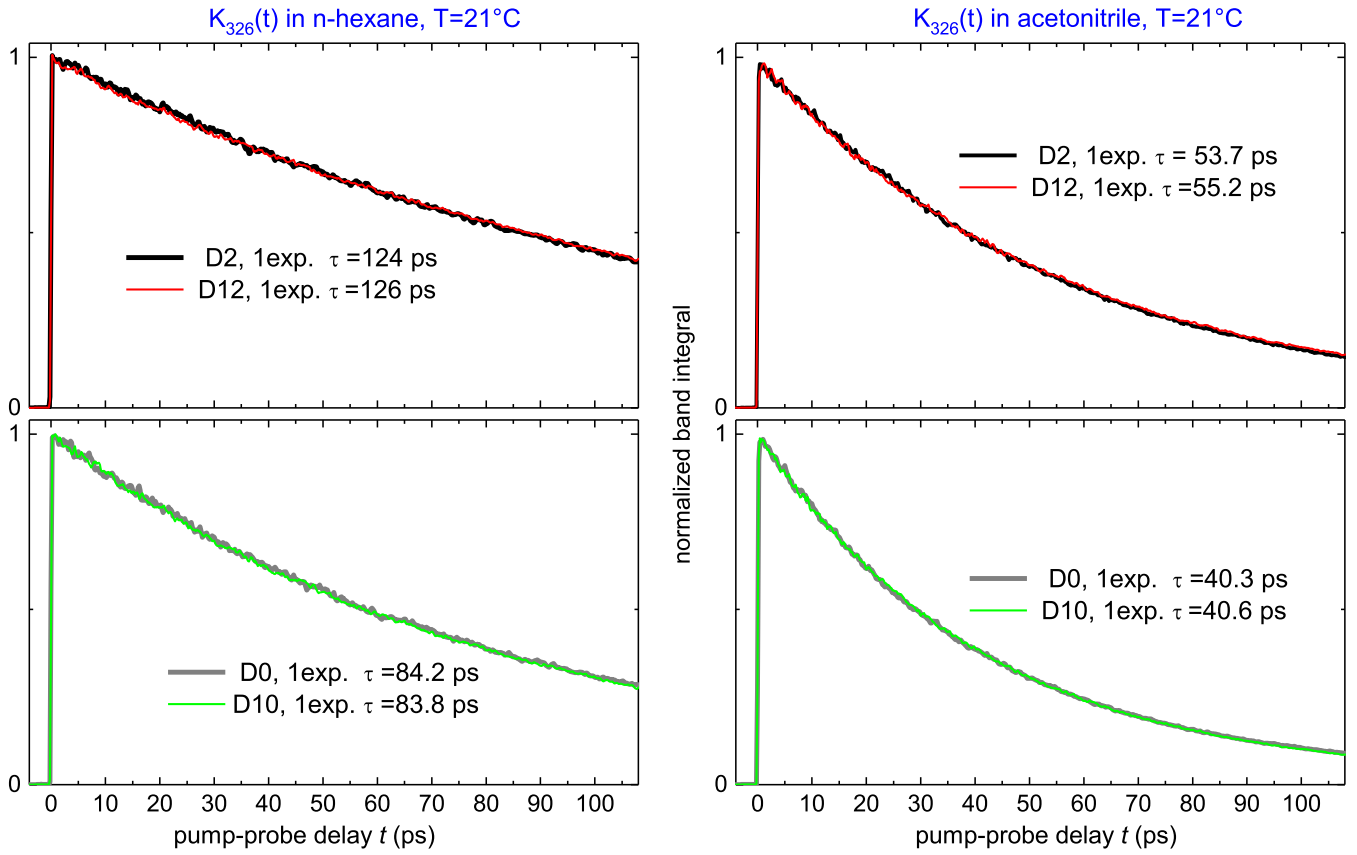

Figure 10. Deuteration effect on the photoisomerization kinetics $K_{326}(t)$ of tS in solution upon λ_{exc} = 326 nm. Here D0 nondeuterated tS, D2 ethylenic deuteration, D10 phenyl deuteration, D12 full deuteration. The decays are monoexponential with time constant τ shown as insert. The kinetics are indistinguishable for D0, D10, and for D2, D12, indicating the same A_S in eq 13a as expected for the collisional isomerization mechanism. The D2 kinetics is slower than the D0 kinetics by factor 1.49 in *n*-hexane and 1.35 in acetonitrile, the effect being due to the different isomerization barrier E_b (see Figure 11).

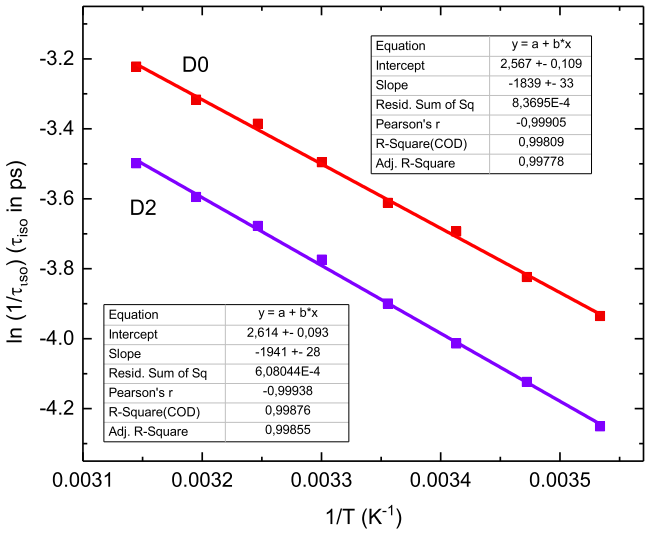

Figure 11. An Arrhenius fit of photoisomerization rate $k_{iso} = A \exp(-E_b/kT_S)$, $A = (A_m+A_S)$, eq 13a, for nondeuterated D0 and deuterated D2 in acetonitrile. The fit results in $A = (13.0 \pm 1.4)$ ps^{-1}, $E_b = (1278 \pm 23)$ cm^{-1} for D0, and $A = (13.6 \pm 1.3)$ ps^{-1}, $E_b = (1349 \pm 19)$ cm^{-1} for D2, that confirms the same collision frequency A_S for D0 and D2, and the different isomerization barrier E_b.

4.3. Different Isomerization Path/Frequency in Solution Compared to Jet/Gas. A fit of photoisomerization kinetics in solution by eq 13 at high excess energy (λ_{exc} = 267 nm for tS, or 285 nm for ttD, Figure 8) allows one to derive the intramolecular contribution A_m not directly accessible in normal measurements with low excess energy, $\lambda_{exc} \approx \lambda_{00}$. The fit results are summarized in Table 8.

Table 8. Solvent A_S and Molecular A_m Contribution to k_{iso} for D0, D2 and ttD

	τ_c (ps)	A_S (ps^{-1})	A_m (ps^{-1})	ν_{iso} (cm^{-1})	E_b (cm^{-1})
D0 he	10	18.0	0.7	23	1518
D0 ac	10	12.9	0.2	7	1280
D2 he	10	17.7	0.3	10	1570
D2 ac	10	13.0	0.1	4	1350
ttD ac	10	13.0	0.1	4	1180

The data in Table 8 reveal the barrier lowering in polar solvent due to the *P*-state stabilization and the kinetic isotope effect of deuteration, the latter being reproducible in the calculations.[53] However, the both effects affect not only E_b but also A_m, that leaves a number of questions.

First, we see a 3-fold drop of A_m in acetonitrile compared to *n*-hexane. If one assumes that $A_m = c\nu_{iso}$ as in eq 1, it can hardly be solvent-dependent since excited tS remains nonpolar before reaching the barrier.[53] Second, there is a 2-fold drop in A_m upon D2 deuteration. One can hardly see, how the ethylenic deuteration would cause such a drop in the twisting frequency, while the effective mass for the twisting motion is mostly due

https://doi.org/10.1021/jacs.4c09134
J. Am. Chem. Soc. 2024, 146, 32463−32478

to the phenyl rings. Furthermore, the estimated ν_{iso} in Table 8 becomes exceedingly low in most cases. In view of that, one may suppose that a simplified picture, with fixed ν_{iso} and remaining normal modes unchanged, is not fully relevant. Perhaps, more exact equations of the transition-state theory need to be invoked, where A_m includes the kT/h factor and the ratio of partition sums of transition state and reactant. Unfortunately, rationalization of the effect of solvent polarity on A_m would still remain problematic. The data in Table 8 may imply that the solvent polarity affects some low-frequency modes in the transition state close to the polar *P*-state, but presently there is no obvious model to explain that.

Consistently with our model, the rate A_S is virtually independent of deuteration, but there is some 1.4-fold drop in A_S between *n*-hexane and acetonitrile, implying that the collisions in acetonitrile activate twisting less efficiently compared to *n*-hexane. In the gas-phase collision theory, the reaction rate is inversely proportional to the square root of the reduced mass of colliding particles. Taking $m_{Ph} = 77$, $m_{he} = 86$, $m_{ac} = 41$, one obtains a factor of 1.2 in favor of *n*-hexane. Thus, the trend in the solvent rate A_S is at least in a qualitative agreement with the proposed model.

4.4. On Restricted IVR and Cooling by Excitation. Restricted IVR has been considered so far as a solution of stilbene photoisomerization problem.[8,14,15,43,47,48,54,55] We briefly discuss this view following a paper by Leitner et al.[48] Their main assumptions are (i) the RRKM rate k_{RRKM} is not achieved in jet because of slow (restricted) IVR; (ii) k_{RRKM} is realized in liquid solution and in high-pressure buffers; (iii) a high frequency reaction mode, $\nu_{iso} = 607$ cm^{-1} for D0, and $\nu_{iso} = 475$ cm^{-1} for D2, is proposed in order to explain the high isomerization rate in solution, and the difference in rate for D0 and D2.

Point (i) contradicts to the Arrhenius dependence of k_{iso} in jet (Figure 7) that shows (a) that k_{RRKM} is consistent with experiment, and (b) suggests that IVR is complete. A strong argument against incomplete IVR was provided by Troe and co-workers[19] with their RRKM calculation over 5 orders of magnitude of the reaction rate in the gas-phase for D2, D10 and D0 (Figures 4 and 5, ref 19). Point (ii) is refuted by the isomerization kinetics in solution at high excess excitation energy (Figure 9); at $T_m(0) = 607$ K the early isomerization rate is similar to the gas-phase rate, but then the low temperature behavior cannot be not reproduced. This implies that the reaction is triggered by a process which is faster than IVR and directly activates the reaction mode (like solvent collisions with the phenyl rings in our model). Next, the assumed high frequency $\nu_{iso} = 607$ cm^{-1} (iii) disagrees with the experiment, $\nu_{iso} = 60$ cm^{-1} for D0 in jet. Furthermore, the assumed different ν_{iso} for D0 and D2 would result in the different rate *A* in solution, contrary to the same $A = 13$ ps^{-1} for D0, D2 in acetonitrile, Figure 11.

An alternative explanation for a slow isomerization rate in jet, compared to solution, was proposed by Pollak and co-workers[45,46] who assumed substantial cooling of the tS molecule upon the 0−0 excitation. Such a cooled molecule would be then heated up by surrounding solvent on a 10 ps scale. The heating should be clearly visible in both TA spectra and kinetics in Figure 2. The ESA band would broaden and shift to the red with increasing temperature $T_m(t)$, and the kinetics would be nonexponential, with a rising component at early time. As no such effects are observed, we conclude that the temperature change by optical cooling is negligible upon the 0−0 excitation.

4.5. Viscosity Effects. The viscosity dependence of the rate k_{iso} was extensively studied[6,7,12,13,16,29,33,37,38] mainly in connection with k_{Kram}, eq 2, in hope to fit experimental kinetics by the Kramers model.[59,60] However, k_{Kram} is closely related to k_{RRKM} corrected for viscosity η. These rates are identical for small η, and proportional to each other for large η, $k_{Kram} \sim k_{RRKM}/\eta$. Thus, their applicability range should be the same. In particular eq 2 is correct for low-pressure gases and small η, when the collisional contribution to k_{iso} is negligible. In high-pressure buffers and in liquid solution, eq 2 cannot be applied alone, and should be replaced by eq 13 with molecular A_m and solvent A_S contribution. The latter is mainly responsible for the viscosity dependence of k_{iso} since $A_S \gg A_m$ in solution. As the theoretical form $A_S(\eta)$ is currently unknown, we restrict ourselves by empirical results.

We have confirmed previously established power dependence $k_{iso} \sim \eta^{-\alpha}$ on viscosity η in *n*-alkanes,[13] with $\alpha = 0.30$ for tS, and $\alpha = 0.35$ for ttD. This can be compared to results by Fleming and co-workers,[13] $\alpha = 0.32$ for tS, and $\alpha = 0.66$ for ttD. We believe that our value for ttD is correct, as the two molecules are quite similar in size and geometry that should result in similar α.

The intramolecular barrier E_{in} in solution is obtained from simultaneous temperature-dependent measurements of rotational and isomerization rates, eqs 7 and 8. By these equations one obtains the viscosity contribution αE_η to the apparent E_b, that gives the inner barrier $E_{in} = (E_b - \alpha E_\eta)$. We believe that this estimate is correct not only for *n*-alkanes but also for other solvents. The result for tS, $E_{in} = 1236$ cm^{-1} (Table 6) can be compared to $E_{in} = 1398$ cm^{-1} in jet. The barrier lowering by 162 cm^{-1} may be explained by the inductive/dispersive stabilization of the polar *P*-state.[69] Previously Saltiel and Sun[16] obtained a smaller value $E_{in} \approx 1000$ cm^{-1} by using their solvent cage model with $\alpha = 0.4$.

Despite the good power dependence $\tau_{iso} \sim \eta^{\alpha}$ in *n*-alkanes (Figure 3), large deviations occur in isoalkanes, cyclohexane and perfluorohexane (Figure 3). This indicates substantial solvent size effects which should be accounted for in theoretical consideration. We have also analyzed the isoviscosity rates[16,17] and shown that they result in increasing barrier E_b and solvent factor A_S with decreasing viscosity η (Figure 6), that seems unphysical. However, more measurements in a wider viscosity range are required to justify this result.

5. CONCLUSIONS

We have discussed a longstanding problem of stilbene photochemistry, the very different photoisomerization rate k_{iso} of *trans*-stilbene in jet/gas and liquid solution, and the applicability of RRKM and Kramers theory to α,ω-diphenylpolienes. We have shown that in jet/gas at collisionless conditions, the RRKM rate $k_{RRKM} = A_m \exp(-E_{in}/kT_m)$ agrees well with experiment. A fit of k_{RRKM} to experimental k_{iso} provides key quantities, reaction frequency $\nu_{iso} = A_m/c = (60 \pm 5)$ cm^{-1} and isomerization barrier $E_{in} = (1398 \pm 26)$ cm^{-1}. However, in compressed buffer gases and in solution, the RRKM or Kramers theory cannot fit the experimental kinetics. In this case the rate should be modified, $k_{iso} = [A_m \exp(-E_b/kT_m) + A_S \exp(-E_b/kT_S)]$, to account for the solvent collisional activation A_S. A possible mechanism behind this term is that solvent collisions with tS or ttD phenyl

https://doi.org/10.1021/jacs.4c09134
J. Am. Chem. Soc. 2024, 146, 32463−32478

rings provide a momentum perpendicular to the molecular plane, thus directly promoting the ethylenic twist, and hence the isomerization. Besides, measurements with high excess vibrational energy, $\lambda_{exc} \ll \lambda_{00}$, allow one to observe the intramolecular part A_m, usually hidden in solution under the much higher A_S contribution. The A_m appears to be different from that in jet/gas and depends on solvent and deuteration pattern. The viscosity dependence of rotational and isomerization rate, $k_R \sim 1/\eta$, $k_{iso} \sim \eta^{-\alpha}$, results in the inner isomerization barrier in solution, $E_{in} = (E_b - \alpha E_\eta) = (1236 \pm 36)$ cm^{-1} for tS, where E_η is the viscosity-associated barrier.

■ ASSOCIATED CONTENT

Supporting Information

The Supporting Information is available free of charge at https://pubs.acs.org/doi/10.1021/jacs.4c09134.

Potential energy surface for stilbene photoisomerization, decay kinetics of ESA and bleach for tS in *n*-hexane and ttD in acetonitrile, geometries and vibrational frequencies for tS and ttD (PDF)

■ AUTHOR INFORMATION

Corresponding Author

Sergey A. Kovalenko − *Department of Chemistry, Humboldt University of Berlin, Berlin 12489, Germany*; orcid.org/0000-0003-4278-9305; Email: skovale@chemie.hu-berlin.de.

Authors

Alexander L. Dobryakov − *N. N. Semenov Federal Research Center of Chemical Physics, Russian Academy of Science, Moscow 119991, Russia*

Daria Schriever − *Department of Physics, Free University of Berlin, Berlin 14195, Germany*

Martin Quick − *Department of Chemistry, Humboldt University of Berlin, Berlin 12489, Germany*

J. Luis Pérez-Lustres − *Department of Physics, Free University of Berlin, Berlin 14195, Germany*

Ilya N. Ioffe − *Department of Chemistry, Lomonosov Moscow State University, Moscow 119991, Russia*

Complete contact information is available at: https://pubs.acs.org/10.1021/jacs.4c09134

Notes

The authors declare no competing financial interest.

■ ACKNOWLEDGMENTS

We thank N.P. Ernsting for help, critical discussions and continuous support at all the stages of this work. We are also grateful to J. Stähler for support and critical comments, and to K. Heyne for support. The research is carried out using the equipment of the shared research facilities of HPC computing resources at Lomonosov Moscow State University.

■ REFERENCES

(1) Saltiel, J. Perdeuteriostilbene. The Role of Phantom States in the cis-trans Photoisomerization of Stilbenes. *J. Am. Chem. Soc.* **1967**, *89*, 1036.

(2) Sumitani, M.; Nakashima, N.; Yoshihara, K.; Nagakura, S. Temperature Dependence of Fluorescence Lifetimes of trans-Stilbene. *Chem. Phys. Lett.* **1977**, *51*, 183.

(3) Orlandi, G.; Siebrand, W. Model for Direct Photoisomerization of Stilbene. *Chem. Phys. Lett.* **1975**, *30*, 352.

(4) Hochstrasser, R. M. Picosecond Processes in the Isomerism of Stilbenes. *Pure Appl. Chem.* **1980**, *52*, 2683.

(5) Greene, B. I.; Hochstrasser, R. M.; Weisman, R. B. Photoproperties of Isolated cis and trans Stilbene Molecules. *Chem. Phys.* **1980**, *48*, 289.

(6) Rothenberger, G.; Negus, D. K.; Hochstrasser, R. M. Solvent Influence on Photoisomerization Dynamics. *J. Chem. Phys.* **1983**, *79*, 5360.

(7) Lee, M.; Holtom, G. R.; Hochstrasser, R. M. Observationof the Kramers Turnover Region in the Isomerism of trans-Stilbene in Fluid Ethane. *Chem. Phys. Lett.* **1985**, *118*, 359.

(8) Khundkar, L. R.; Marcus, R. A.; Zewail, A. H. Unimolecular Reactions at Low Energies and RRKM Behavior: Isomerization and Dissociation. *J. Phys. Chem. A* **1983**, *87*, 2473.

(9) Syage, J. A.; Felker, P. M.; Zewail, A. H. Picosecond Dynamics and Photisomerization of Stilbene in Supersonic beams. II Reacion Rates and Potential Energy Surface. *J. Chem. Phys.* **1984**, *81*, 4706.

(10) Felker, P. M.; Zewail, A. H. Rates of Photoisomerization of trans-Stilbene in Isolated and Solvated Molecules: Experiments on the Deuterium Isotope Effect and RRKM Behavior. *J. Phys. Chem. A* **1985**, *89*, 5402.

(11) Baskin, J. S.; Banares, L.; Pedersen, S.; Zewail, A. H. Femtosecond Real-Time Probing of Reactions. 20. Dynamics of Twisting, Alignment, and IVR in the trans-Stilbene Isomerization Reaction. *J. Phys. Chem. A* **1996**, *100*, 11920.

(12) Courtney, S. H.; Fleming, G. R. Photoisomerization of Stilbene in Low Viscosity Solvents: Comparison of Isolated and Solvated molecules. *J. Chem. Phys.* **1985**, *83*, 215 DOI: 10.1063/1.449811.

(13) Fleming, G. R.; Courtney, S. H.; Balk, M. W. Activated Barrier Crossing: Comparison of Experiment and Theory. *J. Stat. Phys.* **1986**, *42*, 83.

(14) Balk, M. W.; Fleming, G. R. Unimolecular Reactions in Isolated and Collisional Systems: Is the Transition-State Rate an Upper Limit for the Isomerization of Stilbene? *J. Phys. Chem. A* **1986**, *90*, 3975.

(15) Courtney, S. H.; Balk, M. W.; Philips, L. A.; Webb, S. P.; Yang, D.; Levy, D. H.; Fleming, G. R. Unimolecular Reactions in Isolated and Collisional systems: Deuterium Isotope Effect in the Photoisomerization of Stilbene. *J. Chem. Phys.* **1988**, *89*, 6697.

(16) Saltiel, J.; Sun, Y.-P. Intrinsic Potential Energy Barrier for Twisting in the trans-Stilbene S1 State in Hydrocarbon Solvents. *J. Phys. Chem. A* **1989**, *93*, 6246.

(17) Waldeck, D. H. Photoisomerization Dynamics of Stilbenes. *Chem. Rev.* **1991**, *91*, 415.

(18) Meyer, A.; Schroeder, J.; Troe, J. Photoisomerization of trans-Stilbene in Moderately Compressed Gases: Pressure-Dependent Effective Barriers. *J. Phys. Chem. A* **1999**, *103*, 10528.

(19) Schroeder, J.; Steinel, T.; Troe, J. Quantitative Representation of Specific Rate Constants k(E) for the Photoisomerization of Diphenylpolyenes: The Solution of a Longstanding Problem. *J. Phys. Chem. A* **2002**, *106*, 5510.

(20) Iwata, K.; Hamaguchi, H. Picosecond Structural Relaxation of S1 trans-Stilbene in Solution as revealed by Time-Resolved Raman Spectroscopy. *Chem. Phys. Lett.* **1992**, *196*, 462.

(21) Iwata, K.; Ozawa, R.; Hamaguchi, H. Analysis of the Solvent- and Temperature-Dependent Raman Spectral Changes of S1 trans-Stilbene and the Mechanism of the trans to cis Isomerization: Dynamic Polarization Model of Vibrational Dephasing and the CdC Double-Bond Rotation. *J.phys. Chem. A* **2002**, *106*, 3614.

(22) Kovalenko, S. A.; Schanz, R.; Hennig, H.; Ernsting, N. P. Cooling Dynamics of Optically Excited Molecular Probe in Solution from Femtosecond Broadband Transient Absorption Spectroscopy. *J. Chem. Phys.* **2001**, *115*, 3256.

(23) Fuß, W.; Kosmidis, C.; Schmid, W. E.; Trushin, S. A. The lifetime of the Perpendicular Minimum of cis-Stilbene observed by Dissociative Intense-Laser Field Ionization. *Chem. Phys. Lett.* **2004**, *385*, 423.

(24) Kovalenko, S. A.; Dobryakov, A. L.; Ioffe, I.; Ernsting, N. P. Evidence for the Phantom State in Photoinduced cis−trans Isomerization of Stilbene. *Chem. Phys. Lett.* **2010**, *493*, 255.

(25) Berndt, F.; Dobryakov, A. L.; Quick, M.; Mahrwald, R.; Ernsting, N. P.; Lenoir, D.; Kovalenko, S. A. Long-lived Perpendicular Conformation in the Photoisomerization Path of 1,1′-Dimethylstilbene and 1,1′-Diethylstilbene. *Chem. Phys. Lett.* **2012**, *544*, 39.
(26) Dobryakov, A. L.; Ioffe, I.; Granovsky, A. A.; Ernsting, N. P.; Kovalenko, S. A. Femtosecond Raman Spectra of cis-Stilbene and trans-Stilbene with Isotopomers in Solution. *J. Chem. Phys.* **2012**, *137*, No. 244505.
(27) Kovalenko, S. A.; Dobryakov, A. L. On the Excitation Wavelength Dependence and Arrhenius Behavior of Stilbene Isomerization Rates in Solution. *Chem. Phys. Lett.* **2013**, *570*, 56.
(28) Ioffe, I. N.; Quick, M.; Quick, M. T.; Dobryakov, A. L.; Richter, C.; Granovsky, A. A.; Berndt, F.; Mahrwald, R.; Ernsting, N. P.; Kovalenko, S. A. Tuning Stilbene Photochemistry by Fluorination: State Reordering Leads to Sudden Polarization Near the Franck-Condon Region. *J. Am. Chem. Soc.* **2017**, *139*, 15265.
(29) Velsko, S. P.; Fleming, G. R. Photochemical Isomerization in Solution. Photophysics of Diphenylbutadiene. *J. Chem. Phys.* **1982**, *76*, 3553.
(30) Courtney, S. H.; Fleming, G. R. Search for the Kramers Theory Turnover: Photochemical Isomerization at Very Low Viscosity. *Chem. Phys. Lett.* **1984**, *103*, 443.
(31) Courtney, S. H.; Fleming, G. R.; Khundkar, L. R.; Zewail, A. H. Unimolecular Reaction Rates in Solution and in the Isolated Molecule: Comparison of Diphenylbutadiene Nonradiative Decay in Solution and Supersonic Jets. *J. Chem. Phys.* **1984**, *80*, 4559.
(32) Amirav, A.; Sonnenschein, M.; Jortner, J. Interstate Coupling and Dynamics of Excited Singlet States of Isolated Diphenylbutadiene. *Chem. Phys.* **1986**, *102* (102), 305.
(33) Lee, M.; Bain, J.; McCarthy, P. J.; Han, C. H.; Haseltine, J. N.; Smith, A. B., III; R M Hochstrasser, J. Picosecond Photoisomerization and Rotation Reorientation Dynamics in Solution. *Chem. Phys.* **1986**, *85*, 4341.
(34) Allen, M. T.; Whitten, D. G. The Photophysics and Photochemistry of α,ω-Diphenylpolyene Singlet States. *Chem. Rev.* **1989**, *89*, 1691.
(35) Gehrke, C.; Schroeder, J.; Schwarzer, D.; Troe, J.; Voß, F. Photoisomerization of Diphenylbutadiene in Low-Viscosity Nonpolar Solvents: Experimental Manifestations of Multidimensional Kramers Behavior and Cluster Effects. *J. Chem. Phys.* **1990**, *92*, 4805.
(36) Gehrke, C.; Mohrschladt, R.; Schroeder, J.; Troe, J.; Vöhringer, P. Photoisomerization Dynamics of Diphenylbutadiene in Compressed Liquid Alkanes and in Solid Environment. *Chem. Phys.* **1991**, *152*, 45.
(37) Anderton, R. M.; Kauffman, J. F. Photoisomerization Rates of Diphenylbutadiene in n-Alcohols: Dielectric-Dependent Activation Energies Determined via Fits to Kramers Expression. *J. Phys. Chem. A* **1994**, *98*, 12125.
(38) Dahl, K.; Biswas, R.; Maroncelli, M. The Photophysics and Dynamics of Diphenylbutadiene in Alkane and Perfluoroalkane Solvents. *J. Phys. Chem. A* **2003**, *107*, 7838.
(39) Itoh, T. Fluorescence Spectra and the 2Ag level of 1,4-Diphenylbutadiene in Perfluorohexane and Perfluoropentane. *Chem. Phys. Lett.* **2001**, *342*, 550.
(40) Itoh, T.; Numata, Y.; Suzuka, I. Fluorescence Spectra of all trans 1,4-Diphenylbutadiene Obtained by Two-Photon Excitation into 2Ag State. *Chem. Phys. Lett.* **2007**, *445*, 179.
(41) Krohn, O. A.; Quick, M.; Sudarkova, S. M.; Ioffe, I. N.; Richter, C.; Kovalenko, S. A. Photoisomerization Dynamics of trans−trans, cis−trans, and cis−cis Diphenylbutadiene from Broadband Transient Absorption Spectroscopy and Calculations. *J. Chem. Phys.* **2020**, *152*, No. 224305.
(42) Dobryakov, A. L.; Krohn, O. A.; Quick, M.; Ioffe, I. N.; Kovalenko, S. A. Positive and Negative Signal and Line Shape in Stimulated Raman Spectroscopy: Resonance Femtosecond Raman Spectra of Diphenylbutadiene. *J. Chem. Phys.* **2022**, *156*, No. 084304.
(43) Nordholm, S. Photoisomerization of Stilbene − A Theoretical Study of Deuteration Shifts and Limited Internal Vibrational Redistribution. *Chem. Phys.* **1989**, *137*, 109.
(44) Negri, F.; Orlandi, G. Deuterium Isotope Effect on the Photoisomerization Rates of Stilbene: An RRKM Analysis Based on Computed Vibrational Frequencies. *J. Phys. Chem. A* **1991**, *95*, 748.
(45) Gershinsky, G.; Pollak, E. Unimolecular Reactions in the Gas and Liquid Phases: A Possible Resolution to the Puzzles of the trans-Stilbene Isomerization. *J. Chem. Phys.* **1997**, *107*, 812.
(46) Tatchen, J.; Pollak, E. *Ab Initio* Spectroscopy and Photinduced Cooling of the trans-Stilbene Molecule. *J. Chem. Phys.* **2008**, *128*, No. 164303.
(47) Leitner, D. M.; Wolynes, P. G. Quantum Energy Flow During Molecular Isomerization. *Chem. Phys. Lett.* **1997**, *280*, 411.
(48) Leitner, D. M.; Levine, B.; Quenneville, J.; Martinez, T. J.; Wolynes, P. G. Quantum Energy Flow and trans-Stilbene Photoisomerization: Example of a Non-RRKM Reaction. *J. Phys. Chem. A* **2003**, *107*, 10706.
(49) Gagliardi, L.; Orlandi, G.; Molina, V.; Malmqvist, P.-Å.; Roos, B. Theoretical Study of the Lowest ^1B_U States of trans-Stilbene. *J. Phys. Chem. A* **2002**, *106*, 7355.
(50) Improta, R.; Santoro, F. Excited-State Behaviour of trans and cis Isomers of Stilbene and Stiff Stilbene: A TD-DFT Study. *J. Phys. Chem. A* **2005**, *109*, 10058.
(51) Weston, R. E.; Barker, J. R. On Modeling the Pressure-dependent Photoisomerization of trans-Stilbene by Including Slow Intramolecular Vibrational Energy Redistribution. *J. Phys. Chem. A* **2006**, *110*, 7888.
(52) Minezawa, N.; Gordon, M. S. Photoisomerization of Stilbene: A Spin-Flip Density Functional Theory Approach. *J. Phys. Chem. A* **2011**, *115*, 7901.
(53) Ioffe, I. N.; Granovsky, A. A. Photoisomerization of Stilbene: The Detailed XMCQDPT2 Treatment. *J. Chem. Theory Comput.* **2013**, *9*, 4973.
(54) Leitner, D. M. Quantum Ergodicity and Energy Flow in Molecules. *Adv. Phys.* **2015**, *64*, 445.
(55) Leitner, D. M. Molecules and the Eigenstate Thermalization Hypothesis. *Entropy* **2018**, *20*, 673.
(56) Kumpulainen, T.; Lang, B.; Rosspeintner, A.; Vauthey, E. Ultrafast Elementary Photochemical Processes of Organic Molecules in Liquid Solution. *Chem. Rev.* **2017**, *117*, 10826.
(57) Kovalenko, S. A.; Dobryakov, A. L.; Ruthmann, J.; Ernsting, N. P. Femtosecond Spectroscopy of Condensed Phases with Chirped Supercontinuum Probing. *Phys. Rev. A* **1999**, *59*, 2369.
(58) Marcus, R. A. Unimolecular Dissociations and Free Radical Recombination Reactions. *J. Chem. Phys.* **1952**, *20*, 359.
(59) Kramers, H. A. Brownian Motion in a Field of Force and the Diffusion Model of Chemical Reactions. *Physica* **1940**, *7*, 284.
(60) Hänggi, P.; Talkner, P.; Borkovec, M. Reaction-Rate Theory: Fifty Years after Kramers. *Rev. Mod. Phys.* **1990**, *62*, 251.
(61) Aldaz, C. R.; Martinez, T. J.; Zimmerman, P. M. The Mechanics of the Bicycle Pedal Photoisomerization in Crystalline cis,cis-1,4-Diphenyl-1,3-butadiene. *J. Phys. Chem. A* **2020**, *124*, 8897.
(62) Granovsky, A. A. *Firefly v. 8.2*, March 2024, http://classic.chem.msu.su/gran/firefly/index.html.
(63) Schmidt, M. W.; Baldridge, K. K.; Boatz, J. A.; Elbert, S. T.; Gordon, M. S.; Jensen, J. H.; Koseki, S.; Matsunaga, N.; Nguyen, K. A.; Su, S.; Windus, T. L.; Dupuis, M.; Montgomery, J. A. General Atomic and Molecular Electronic Structure System. *J. Comput. Chem.* **1993**, *14*, 1347.
(64) Granovsky, A. A. Perturbation Theory Extended Multi-configuration Quasi-degenerate Perturbation Theory: The New Approach to Multi-state Multi-reference Perturbation Theory. *J. Chem. Phys.* **2011**, *134*, No. 214113.
(65) Moreno, J.; Dobryakov, A. L.; Ioffe, I. N.; Granovsky, A. A.; Hecht, S.; Kovalenko, S. A. Broadband Transient Absorption Spectroscopy with 1- and 2-photon Excitations: Relaxation Paths and Cross Sections of a Triphenylamine Dye in Solution. *J. Chem. Phys.* **2015**, *143*, No. 024311.
(66) Englman, R.; Jortner, J. The Energy Gap Low for Radiationless Transitions in Large Molecules. *Mol. Phys.* **1970**, *18*, 145.

https://doi.org/10.1021/jacs.4c09134
J. Am. Chem. Soc. 2024, 146, 32463−32478

(67) Jang, S. J. A Simple Generalization of the Energy Gap Law for Nonradiative Processes. *J. Chem. Phys.* **2021**, *155*, No. 164106.
(68) Quick, M. T.; Quick, M.; Ioffe, I. N.; Richter, C.; Mahrwald, R.; Druzhinin, S.; Kovalenko, S. A. Transient Rotamerism and Photoisomerization Dynamics of trans- and cis-Naphthylstilbene. *J. Phys. Chem. B* **2020**, *124*, 1049.
(69) Mataga, N.; Kubota, T. *Molecular Interactions and Electronic Spectra*; Marcel Dekker, 1970.
(70) Saltiel, J.; Waller, A. S.; Sears, D. F.; Garrett, C. Z. Fluorescence Quantum Yield of trans-Stilbene d0 and d2 in n-Hexane and n-Teradecane. Medium and Deuterium Isotope Effects on Decay Processes. *J. Phys. Chem. A* **1993**, *97*, 2516.

https://doi.org/10.1021/jacs.4c09134
J. Am. Chem. Soc. 2024, 146, 32463−32478